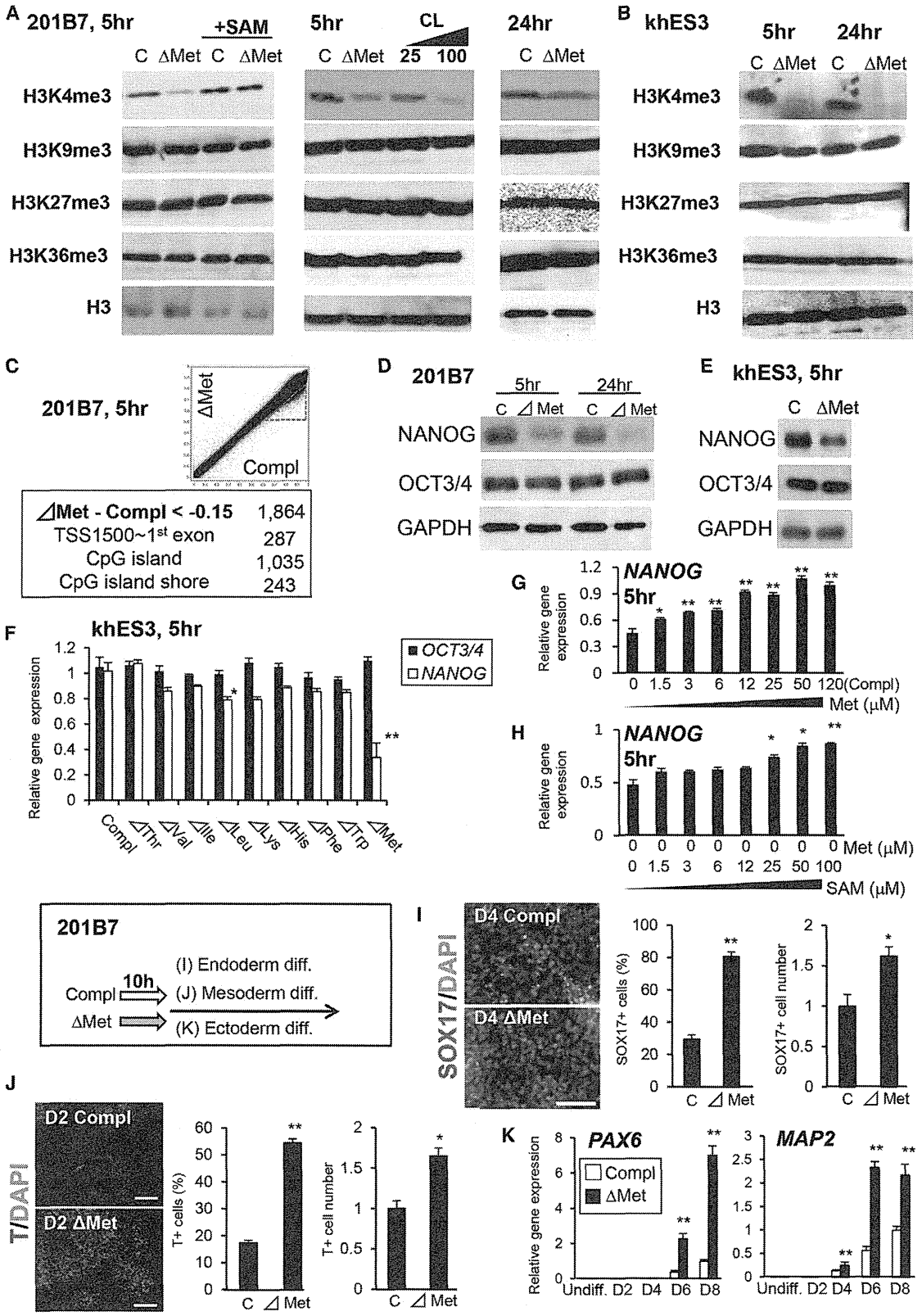

Figure 5. Short-Term Met Deprivation Triggers Histone and DNA Demethylation and Potentiates Differentiation into the Three Germ Layers

(A and B) Histone H3 methylation was examined in undifferentiated 201B7 (A) and khES3 (B) cells cultured in Met-deprived (ΔMet) or control media (C) for 5 or 24 hr. SAM supplementation (100 μM) in Met-deprived media (ΔMet+SAM) reversed demethylation of H3K4me3. Cycloleucine (100 mM) decreased H3K4me3 levels.

(legend continued on next page)

salvage pathway can replenish SAM. However, if Met depletion is prolonged and cells are not exposed to differentiation signals, the Met cycle eventually stops, and human ESCs/iPSCs undergo apoptosis.

Upon Met deprivation, cells halted excretion of Hcy and began to utilize SAM or MTA, resulting in reduced $[SAM]_i$ and $[MTA]_i$, a rapid response observed at 5 hr. *MAT2A* was upregulated to convert Met to SAM and restored the reduced $[SAM]_i$ 24 hr after Met deprivation. These events, such as salvage pathway activation and cessation of Hcy excretion, are stress responses of human ESCs/iPSCs revealed in this study. The pluripotent stem cells developed regulatory systems to maintain $[SAM]_i$ at constant levels. We also found that SAM supplementation rescued the apoptosis induced by Met deprivation, and supplementation of SAM, MTA, or Hcy rescued the impaired cell survival at a potency of SAM > MTA > Hcy. *MAT2A/MAT2B* knockdown or cycloleucine addition, but not *SMS* knockdown, phenocopied Met depletion and resulted in growth inhibition. Because cycloleucine specifically reduces $[SAM]_i$, but not $[Met]_i$, SAM, but not Met, is therefore essential for survival of undifferentiated human ESCs/iPSCs.

SAM is a major methyl donor during methyl transfer reactions, including histone or DNA methylation. Histone methylation contributes to chromatin remodeling as well as transcriptional activity (Berger, 2007). SAM functions as a sensor for Met metabolism, with a rapid decrease in $[SAM]_i$ inducing H3K4me3 and DNA demethylation, as well as decreased NANOG expression and p53-p38 pathway activation. Met deprivation rapidly poised human ESCs/iPSCs for differentiation. However, prolonged exposure to Met deprivation for 24 hr or more in the absence of appropriate differentiation signals caused the cells to undergo an irreversible change, such as prolonged G0/G1 arrest and decreased self-renewal, thus triggering apoptosis. When deprival of Met was performed during mid-stage differentiation, residual undifferentiated cells were eliminated, and overall differentiation efficiency was increased. Therefore, this knowledge is useful and applicable to eliminate variability in differentiation efficiency among cell lines and promote differentiation into specific lineages. Human iPSCs are reportedly dependent on oleate; an inhibitor of oleate synthesis shows cytotoxicity and may selectively eliminate human iPSCs (Ben-David et al., 2013). Cardiomyocytes and noncardiomyocytes from mouse and human ESCs/iPSCs differ markedly in glucose and lactate metabolism; thus, cardiomyocytes can be obtained at a high purity during large-scale purification by culture in glucose-free media (Tohyama et al., 2013). However, culture in glucose-free media did not potentiate differentiation, which differs from our present results regarding short-term Met deprivation.

While methylation of H3K4 is generally associated with activation of transcription, H3K9 and H3K27 are repressive epigenetic markers. In ESCs, simultaneous methylation of H3K4 and H3K27 is associated with the undifferentiated state, where a gene may be poised to be either fully activated or repressed (Bernstein et al., 2006). Here, decreased trimethylation of H3K4 (H3K4me3) resulting from Met deprivation suggests that Met metabolism might function in the regulation of self-renewal of pluripotent stem cells through epigenetic marking at H3K4me3 (Ang et al., 2011). Previously, mouse ESCs were reported to be in a high-flux state requiring Thr to maintain cell-cycle progression (Wang et al., 2009). In mouse ESCs, rapid conversion of Thr to Gly by Tdh is suggested to provide 5-methyltetrahydrofolate (5mTHF) needed for recycling SAH to SAM; thus, Thr deprivation caused a reduction in SAM, which then triggered demethylation of H3K4me3 and H3K4me2 (Shyh-Chang et al., 2013). In humans, the *TDH* gene is an expressed pseudogene (Edgar, 2002). Human ESCs/iPSCs directly generate SAM from Met. Therefore, mouse and human ESCs/iPSCs utilize similarly the Met pathway for maintaining their pluripotent state in principal. Met metabolism directly regulates SAM levels, and SAM reduction triggered demethylation of H3K4me3 (but not H3K9me3, H3K27me3, or H3K36me3) specifically, the mechanism of which remains unknown.

Evidence suggests that self-renewal and pluripotency are closely linked to cell-cycle regulation in pluripotent stem cells and that NANOG plays a role in the G1-to-S transition through direct binding of *CDK6* and *CDC25A* (Zhang et al., 2009). The high self-renewal rate is considered essential for maintaining ESC identity, and cell-cycle arrest is sufficient to drive human ESCs toward irreversible differentiation (Ruiz et al., 2011). Deletion of p53 in mouse cells or silencing of p53 in human somatic cells increases the reprogramming efficiency (Kawamura et al., 2009). p53 induces differentiation by directly suppressing NANOG expression in mouse ESCs (Lin et al., 2005). Our results showed that Met deprivation triggered decreased expression of NANOG, but not OCT3/4. NANOG is a member of the core transcription circuit required for ESCs to maintain pluripotency. While NANOG is actively downregulated during differentiation, OCT3/4 is downregulated when the later lineage choice occurs (Iovino and Cavalli, 2011). Our present results suggest that the Met metabolism is responsible for regulation of cell-cycle progression and maintenance of pluripotency of human ESCs/iPSCs versus differentiation or apoptosis through the p53-p38 signaling pathway. Activation of p53 signaling was observed specifically under conditions of Met deprivation but was not seen upon deprivation of other amino acids, and p53-p38 accumulation was halted by the addition of SAM.

(C) DNA methylation profiles in undifferentiated 201B7 cells cultured in complete medium (x axis) and Met-deprived medium (y axis) for 5 hr. The number of probes with greater than 15% reduction in DNA methylation under Met deprivation are shown.
(D and E) Short-term Met deprivation (5 hr) downregulated NANOG expression in 201B7 (D) and khES3 (E) cells.
(F) Real-time PCR analysis of *NANOG* and *OCT3/4* in khES3 cells in complete or amino acid-deprived media for 5 hr.
(G and H) *NANOG* expression increased with increasing Met (G) or SAM (H) concentration in the media.
(I–K) Human iPSCs cultured in Met-deprived conditions showed an elevated differentiation into the definitive endoderm (I), mesoderm (J), and ectoderm (K), as shown by expression of the endoderm marker SOX17 (I), early mesoderm marker T (J), *PAX*, or *MAP2* (K) by immunohistochemical (I and J) or real-time PCR (K) analyses. Cells were pretreated with complete medium (I and J, left bars; K, open bars) or Met-deprived media (I and J, right bars; K, black bars) before differentiation. Error bars represent SEM (n = 3). Student's t test; *$p < 0.05$ and **$p < 0.01$. Scale bar, 100 μm.

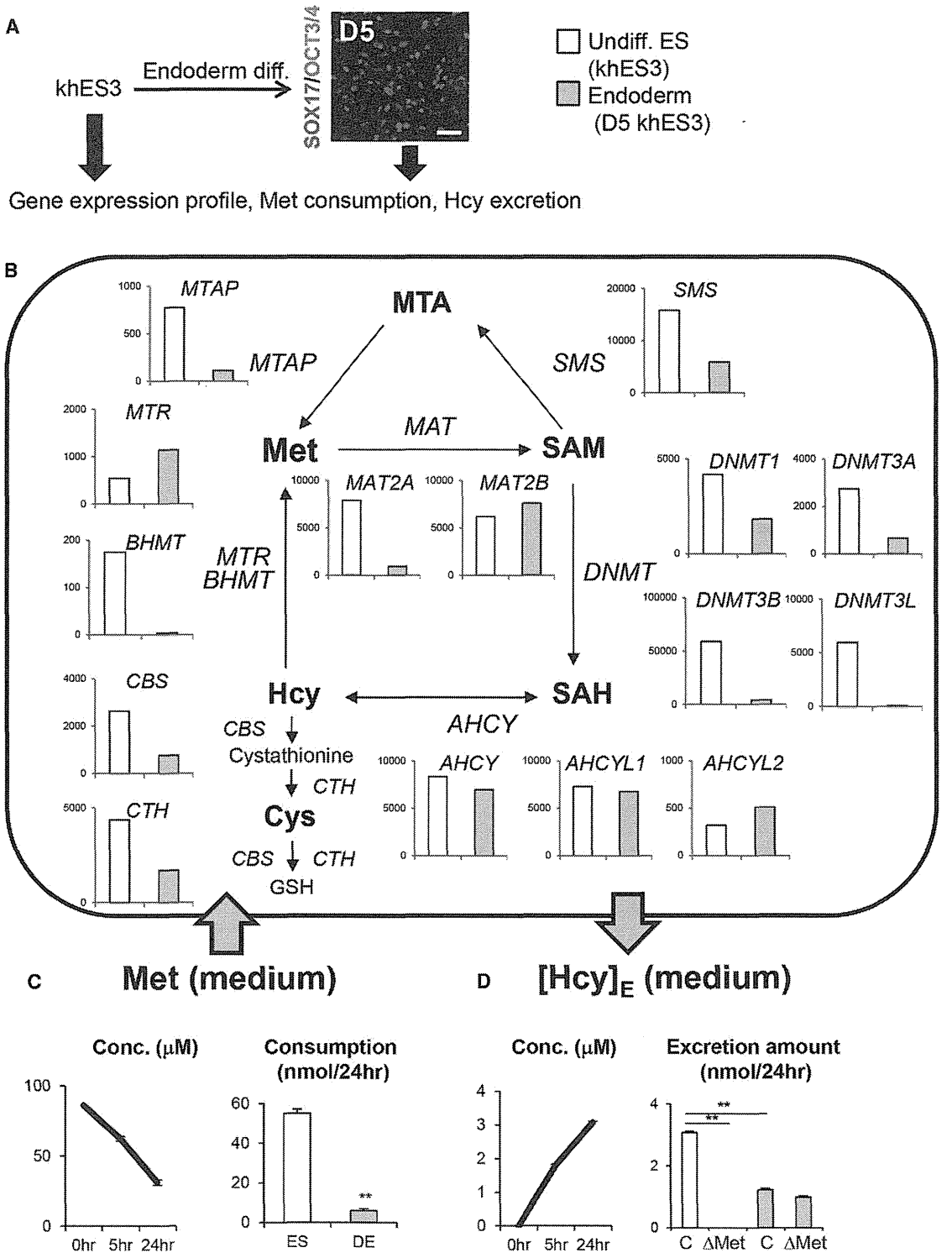

Figure 6. Undifferentiated Human ESCs Are in a High-Met Metabolic State Compared with Definitive Endoderm Cells

(A) Schematic drawings of the experimental design to determine differences in Met metabolism between undifferentiated ESCs and definitive endoderm cells. Endoderm cells differentiated for 5 days expressed SOX17, but not OCT3/4.

(B) Signal intensity of Met cycle-related genes in undifferentiated (undiff) and differentiated khES3 cells on differentiation day 5 (D5) toward the definitive endoderm analyzed by microarray.

(legend continued on next page)

SAM has been reported to act as a stress sensor in malignant cells (Lin et al., 2014). P53 is also known to trigger various stress responses (Kruse and Gu, 2009). We found that 5 hr Met deprivation in khES3 cells triggered a 27-fold increase in the expression of *EGR1*, a transcription factor that upregulates *p53* (Baron et al., 2006), or a 33-fold increase in *DHRS2*, a gene that inhibits Mdm2 and stabilizes p53 protein (Deisenroth et al., 2010). Therefore, Egr1 and DHRS2 are candidate molecules that mediate upregulation of p53 triggered by SAM limitation. However, the exact molecular mechanism linking SAM and p53 still awaits future investigations.

Taken together, our data indicate that Met deprivation results in a rapid decrease in $[SAM]_i$, triggering activation of p53-p38 signaling, reducing NANOG expression, and poising human iPSC/ESCs for differentiation. The cells endured short-term Met deprivation by replenishing the $[Met]_i$ pool with the salvage Met pathway, which was then metabolized to replenish SAM. However, during prolonged Met deprivation, the continued absence of Met metabolism led to cell-cycle arrest and apoptosis. These results are consistent with the data from previous studies indicating that p53 is a barrier to reprogramming and that decreasing p53 protein levels increases the efficiency of reprogramming (Banito et al., 2009; Kawamura et al., 2009). In conclusion, we demonstrated the importance of SAM in Met metabolism in regulating p53 signaling and its relationship with pluripotency, cell survival, and differentiation of human ESCs/iPSCs. Our findings can be utilized to eliminate undifferentiated pluripotent cells in culture and may be useful for future applications in regenerative medicine.

EXPERIMENTAL PROCEDURES

Cell Culture and Reagents

Human ESCs were approved by Kumamoto University's Institutional Review Board, following the hESC guidelines of the Japanese government. Undifferentiated human ESCs (khES1, khES3) (Suemori et al., 2006) and iPSCs (201B7, 253G1) (Takahashi et al., 2007) were maintained as described (Shiraki et al., 2008a). For feeder-free culture, ESCs/iPSCs were cultured on matrigel-coated dish with feeder-free culture media ReproFF (ReproCELL). For Met deprivation with undifferentiated cells, cells were cultured with human ESC/iPSC maintenance medium CSTI-7 (Cell Science & Technology Institute; CSTI) (Furue et al., 2008) or Met-deprived CSTI-7 medium. Met, Hcy, Cys, SAM, MTA, cycloleucine, and SAH were purchased from Sigma-Aldrich. SB239063 was purchased from Calbiochem. Methods of endoderm, mesoderm, or ectoderm differentiation, and gene knockdown examination, are described in Supplemental Experimental Procedures.

Real-Time PCR, Immunocytochemistry, and Western Blot Analysis

Real-time PCR, immunocytochemistry, and western blot were performed as previously described (Shiraki et al., 2011). Primer sequences and antibody information are shown in Tables S2 and S3, respectively. In immunocytochemical analysis, positive cells versus total cells (DAPI-positive cells) were quantified using ImageXpress Micro cellular imaging system (Molecular Devices).

Measurement of Met, SAM, SAH, MTA, and Hcy

Measurement of methionine, SAM, SAH, MTA, and Hcy was performed using ultra-high-performance liquid chromatography equipped with tandem mass spectrometry, TQD (UPLC-MS/MS; Waters) based on a previous report (Jiang et al., 2009). Separation was achieved using an ACQUITY UPLC BEH C18 column. Briefly, cells were lysed using three cycles of freeze/thaw in 50% methanol. Samples were deproteinized using 33% acetonitrile and evaporated completely. Pellets were dissolved in 10 mM HCl, followed by filtration using 0.22 μm polyvinylidene fluoride (PVDF) filter (Millipore) and diluted with equal volumes of either 50 mM Tris-HCl (pH 8.8) with 100 μm dithiothreitol (DTT) for Met, SAM, and SAH or 20 mM formic acid for MTA. For Hcy analysis in the media, cultured media were collected and incubated for 10 min at 37°C with 10 mM DTT to obtain total Hcy secreted from the cells. Media were deproteinized using 50% acetonitrile, followed by filtration, and then diluted with equal volumes of 50 mM Tris-HCl (pH 8.8). Each sample was injected, and concentrations were calculated based on the standard curve obtained from serial dilution of standard solution for each metabolite.

Microarray Analysis

Affymetrix H133 Plus 2.0 series probe array (GeneChip) was used. Expression analysis was performed using the Subio Platform (Subio).

Cell-Cycle Analysis

Fixed cells were stained with DAPI and anti-phospho Histone H3 Ser10 (pH3; Millipore). Images were acquired on the ImageXpress Micro and analyzed using the Cell Cycle Application Module (Molecular Devices).

Apoptosis Assay

Apoptosis was detected by the TUNEL method using an In Situ Cell Death Detection Kit (Roche).

Measurement of Cell Proliferation

Cell proliferation was measured by the incorporation of EdU into genomic DNA during the S phase of the cell cycle, using Click-iT EdU Kit (Invitrogen).

Functional Assays for Hepatocytes

Albumin secretion assay was performed as described (Shiraki et al., 2011). Cryopreserved human hepatocytes (Invitrogen) cultured 24 hr on collagen I coated plates with hepatocyte maintenance medium (Invitrogen) were used as positive controls.

Methylation Profiling

Methylation profiling analysis was performed as described (Nagae et al., 2011). Methylation status was analyzed using the Human Methylation 450 BeadChip (Illumina).

Statistical Analysis

Error bars represent SEM. The significance of differences between two groups was analyzed by Student's t test and presented as $^*p < 0.05$ or $^{**}p < 0.01$.

ACCESSION NUMBERS

Microarray data have been deposited under Gene Expression Omnibus (GEO) accession number GSE55285.

SUPPLEMENTAL INFORMATION

Supplemental Information includes Supplemental Experimental Procedures, four figures, and three tables and can be found with this article online at http://dx.doi.org/10.1016/j.cmet.2014.03.017.

AUTHOR CONTRIBUTIONS

N.S. and Y.S. designed the experiments and performed cellular and biochemical analyses to check the effect of Met in differentiation stages. N.S.

(C) Time-dependent changes in Met concentration 5 or 24 hr after culture in complete media (left). Met consumption at 24 hr in undifferentiated or endoderm cells (right).

(D) Time-dependent excretion of Hcy 5 or 24 hr after culture in complete media. Excreted Hcy ($[Hcy]_E$) at 24 hr in undifferentiated or endoderm cells grown in complete or Met-deprived media. Error bars represent SEM (n = 3). Student's t test; $^{**}p < 0.01$. Scale bar, 100 μm. Open bars, undifferentiated cells; gray bars, definitive endoderm.

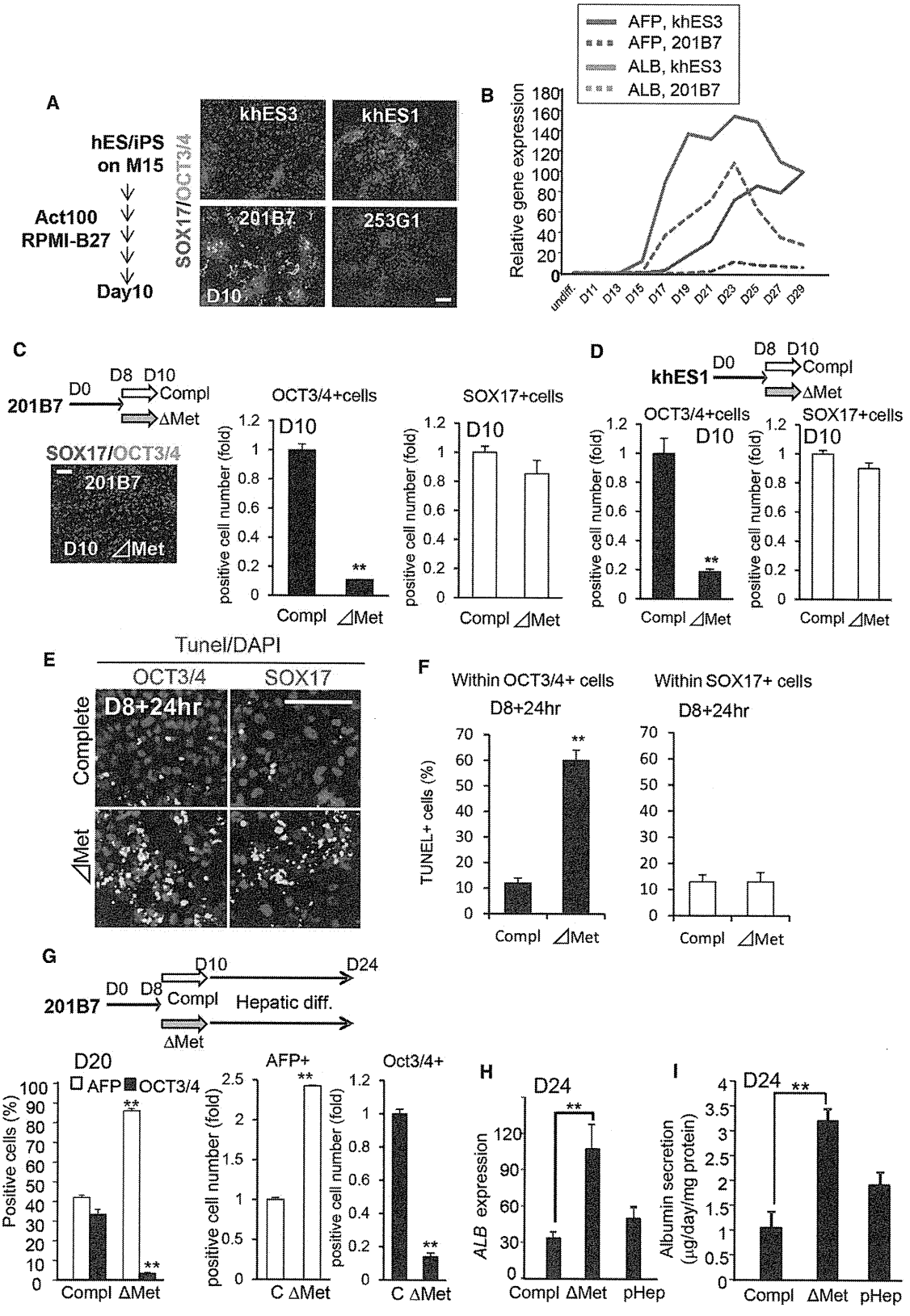

(legend on next page)

performed cellular and biochemical analyses to check the effect of Met in the undifferentiation stage and wrote the paper. T.T. handled the collection and assembly of data. F.O. and M.M. performed the measurement of Met-cycle metabolites. G.N. and H.A. performed the analysis of global DNA methylation. K.K. provided technical advice and helpful discussions. F.E. conceived the study and provided technical advice and financial support. S.K. conceived the study and design, wrote the paper, interpreted results, provided financial support, and finalized the manuscript.

ACKNOWLEDGMENTS

We thank Drs. Norio Nakatsuji and Hirofumi Suemori (Kyoto University) for providing khES1 and khES3 cells and Dr. Shinya Yamanaka (Kyoto University) for providing 201B7 and 253G1 iPSC lines. We thank Ms. Nigar Sultana, Akiko Harada, and the members of the Gene Technology Center at Kumamoto University for their technical assistance. This work was supported by a grant from the National Institute of Biomedical Innovation (to N.S.); the NEXT Program (to S.K.) by the Japanese Society for the Promotion of Science (JSPS); and a grant from the Project for Realization of Regenerative Medicine from the Ministry of Education, Culture, Sports, Science and Technology (MEXT) Japan (to S.K. and F.E.). This work was also supported in part by the Program for Leading Graduate Schools "HIGO (Health life science; Interdisciplinary and Glocal Oriented) Program" (to S.K.), from MEXT. S.K. is a member of the Program for Leading Graduate Schools "HIGO."

Received: September 22, 2013
Revised: January 9, 2014
Accepted: March 11, 2014
Published: April 17, 2014

REFERENCES

Alexander, P.B., Wang, J., and McKnight, S.L. (2011). Targeted killing of a mammalian cell based upon its specialized metabolic state. Proc. Natl. Acad. Sci. USA *108*, 15828–15833.

Ang, Y.S., Tsai, S.Y., Lee, D.F., Monk, J., Su, J., Ratnakumar, K., Ding, J., Ge, Y., Darr, H., Chang, B., et al. (2011). Wdr5 mediates self-renewal and reprogramming via the embryonic stem cell core transcriptional network. Cell *145*, 183–197.

Armstrong, L., Tilgner, K., Saretzki, G., Atkinson, S.P., Stojkovic, M., Moreno, R., Przyborski, S., and Lako, M. (2010). Human induced pluripotent stem cell lines show stress defense mechanisms and mitochondrial regulation similar to those of human embryonic stem cells. Stem Cells *28*, 661–673.

Banito, A., Rashid, S.T., Acosta, J.C., Li, S., Pereira, C.F., Geti, I., Pinho, S., Silva, J.C., Azuara, V., Walsh, M., et al. (2009). Senescence impairs successful reprogramming to pluripotent stem cells. Genes Dev. *23*, 2134–2139.

Baron, V., Adamson, E.D., Calogero, A., Ragona, G., and Mercola, D. (2006). The transcription factor Egr1 is a direct regulator of multiple tumor suppressors including TGFbeta1, PTEN, p53, and fibronectin. Cancer Gene Ther. *13*, 115–124.

Ben-David, U., Gan, Q.F., Golan-Lev, T., Arora, P., Yanuka, O., Oren, Y.S., Leikin-Frenkel, A., Graf, M., Garippa, R., Boehringer, M., et al. (2013). Selective elimination of human pluripotent stem cells by an oleate synthesis inhibitor discovered in a high-throughput screen. Cell Stem Cell *12*, 167–179.

Berger, S.L. (2007). The complex language of chromatin regulation during transcription. Nature *447*, 407–412.

Bernstein, B.E., Mikkelsen, T.S., Xie, X., Kamal, M., Huebert, D.J., Cuff, J., Fry, B., Meissner, A., Wernig, M., Plath, K., et al. (2006). A bivalent chromatin structure marks key developmental genes in embryonic stem cells. Cell *125*, 315–326.

Boheler, K.R. (2009). Stem cell pluripotency: a cellular trait that depends on transcription factors, chromatin state and a checkpoint deficient cell cycle. J. Cell. Physiol. *221*, 10–17.

Bruhat, A., Jousse, C., Wang, X.Z., Ron, D., Ferrara, M., and Fafournoux, P. (1997). Amino acid limitation induces expression of CHOP, a CCAAT/enhancer binding protein-related gene, at both transcriptional and post-transcriptional levels. J. Biol. Chem. *272*, 17588–17593.

Deisenroth, C., Thorner, A.R., Enomoto, T., Perou, C.M., and Zhang, Y. (2010). Mitochondrial Hep27 is a c-Myb target gene that inhibits Mdm2 and stabilizes p53. Mol. Cell. Biol. *30*, 3981–3993.

Edgar, A.J. (2002). The human L-threonine 3-dehydrogenase gene is an expressed pseudogene. BMC Genet. *3*, 18.

Facucho-Oliveira, J.M., and St John, J.C. (2009). The relationship between pluripotency and mitochondrial DNA proliferation during early embryo development and embryonic stem cell differentiation. Stem Cell Rev. *5*, 140–158.

Finkelstein, J.D. (1990). Methionine metabolism in mammals. J. Nutr. Biochem. *1*, 228–237.

Folmes, C.D., Nelson, T.J., Martinez-Fernandez, A., Arrell, D.K., Lindor, J.Z., Dzeja, P.P., Ikeda, Y., Perez-Terzic, C., and Terzic, A. (2011). Somatic oxidative bioenergetics transitions into pluripotency-dependent glycolysis to facilitate nuclear reprogramming. Cell Metab. *14*, 264–271.

Furue, M.K., Na, J., Jackson, J.P., Okamoto, T., Jones, M., Baker, D., Hata, R., Moore, H.D., Sato, J.D., and Andrews, P.W. (2008). Heparin promotes the growth of human embryonic stem cells in a defined serum-free medium. Proc. Natl. Acad. Sci. USA *105*, 13409–13414.

Goll, M.G., and Bestor, T.H. (2005). Eukaryotic cytosine methyltransferases. Annu. Rev. Biochem. *74*, 481–514.

Halim, A.B., LeGros, L., Geller, A., and Kotb, M. (1999). Expression and functional interaction of the catalytic and regulatory subunits of human methionine adenosyltransferase in mammalian cells. J. Biol. Chem. *274*, 29720–29725.

Iovino, N., and Cavalli, G. (2011). Rolling ES cells down the Waddington landscape with Oct4 and Sox2. Cell *145*, 815–817.

Iwashita, H., Shiraki, N., Sakano, D., Ikegami, T., Shiga, M., Kume, K., and Kume, S. (2013). Secreted cerberus1 as a marker for quantification of definitive endoderm differentiation of the pluripotent stem cells. PLoS ONE *8*, e64291.

Jiang, Z., Liang, Q., Luo, G., Hu, P., Li, P., and Wang, Y. (2009). HPLC-electrospray tandem mass spectrometry for simultaneous quantitation of eight plasma aminothiols: application to studies of diabetic nephropathy. Talanta *77*, 1279–1284.

Kajiwara, M., Aoi, T., Okita, K., Takahashi, R., Inoue, H., Takayama, N., Endo, H., Eto, K., Toguchida, J., Uemoto, S., and Yamanaka, S. (2012). Donor-dependent variations in hepatic differentiation from human-induced pluripotent stem cells. Proc. Natl. Acad. Sci. USA *109*, 12538–12543.

Figure 7. Met Deprivation Potentiates Hepatic Differentiation

(A) khES1, khES3, 201B7, and 253G1 cells were subjected to endodermal differentiation using M15 feeder cells (Shiraki et al., 2008a; Umeda et al., 2013). SOX17 (red) and OCT3/4 (green) expression was detected by immunocytochemistry.

(B) *AFP* (red) or *ALB* (blue) mRNA expression was detected by real-time PCR. Expression in khES3 (solid lines) or 201B7 cells (broken lines).

(C and D) Impact of Met deprivation on the remaining $OCT3/4^+$ undifferentiated cells (black bars) or $SOX17^+$ definitive endoderm cells (open bars) derived from 201B7 cells (C) or khES1 cells (D).

(E) Fluorescent image of TUNEL staining.

(F) Quantitative analysis of TUNEL-positive cells.

(G–I) The impact of Met deprivation on hepatic differentiation. (G) Proportions and number of AFP^+ cells (open bars) or $OCT3/4^+$ cells (black bars) in complete or Met-deprived media. (H and I) Upon Met deprivation, increased *ALB* expression (H) and ALB secretion on D24 (I) were observed. pHep, primary human hepatocytes. Error bars represent SEM (n = 3). Significant differences were determined by Student's t test; $^{**}p < 0.01$. Scale bar, 100 μm.

Kawamura, T., Suzuki, J., Wang, Y.V., Menendez, S., Morera, L.B., Raya, A., Wahl, G.M., and Izpisúa Belmonte, J.C. (2009). Linking the p53 tumour suppressor pathway to somatic cell reprogramming. Nature *460*, 1140–1144.

Kruse, J.P., and Gu, W. (2009). Modes of p53 regulation. Cell *137*, 609–622.

Lin, T., Chao, C., Saito, S., Mazur, S.J., Murphy, M.E., Appella, E., and Xu, Y. (2005). p53 induces differentiation of mouse embryonic stem cells by suppressing Nanog expression. Nat. Cell Biol. *7*, 165–171.

Lin, D.W., Chung, B.P., and Kaiser, P. (2014). S-adenosylmethionine limitation induces p38 mitogen-activated protein kinase and triggers cell cycle arrest in G1. J. Cell Sci. *127*, 50–59.

Lu, S.C., and Mato, J.M. (2008). S-Adenosylmethionine in cell growth, apoptosis and liver cancer. J. Gastroenterol. Hepatol. *23* (*Suppl 1*), S73–S77.

Nagae, G., Isagawa, T., Shiraki, N., Fujita, T., Yamamoto, S., Tsutsumi, S., Nonaka, A., Yoshiba, S., Matsusaka, K., Midorikawa, Y., et al. (2011). Tissue-specific demethylation in CpG-poor promoters during cellular differentiation. Hum. Mol. Genet. *20*, 2710–2721.

Ogaki, S., Shiraki, N., Kume, K., and Kume, S. (2013). Wnt and Notch signals guide embryonic stem cell differentiation into the intestinal lineages. Stem Cells *31*, 1086–1096.

Osafune, K., Caron, L., Borowiak, M., Martinez, R.J., Fitz-Gerald, C.S., Sato, Y., Cowan, C.A., Chien, K.R., and Melton, D.A. (2008). Marked differences in differentiation propensity among human embryonic stem cell lines. Nat. Biotechnol. *26*, 313–315.

Oyadomari, S., and Mori, M. (2004). Roles of CHOP/GADD153 in endoplasmic reticulum stress. Cell Death Differ. *11*, 381–389.

Ruiz, S., Panopoulos, A.D., Herrerías, A., Bissig, K.D., Lutz, M., Berggren, W.T., Verma, I.M., and Izpisua Belmonte, J.C. (2011). A high proliferation rate is required for cell reprogramming and maintenance of human embryonic stem cell identity. Curr. Biol. *21*, 45–52.

Shi, Y. (2007). Histone lysine demethylases: emerging roles in development, physiology and disease. Nat. Rev. Genet. *8*, 829–833.

Shiraki, N., Umeda, K., Sakashita, N., Takeya, M., Kume, K., and Kume, S. (2008a). Differentiation of mouse and human embryonic stem cells into hepatic lineages. Genes Cells *13*, 731–746.

Shiraki, N., Yoshida, T., Araki, K., Umezawa, A., Higuchi, Y., Goto, H., Kume, K., and Kume, S. (2008b). Guided differentiation of embryonic stem cells into Pdx1-expressing regional-specific definitive endoderm. Stem Cells *26*, 874–885.

Shiraki, N., Yamazoe, T., Qin, Z., Ohgomori, K., Mochitate, K., Kume, K., and Kume, S. (2011). Efficient differentiation of embryonic stem cells into hepatic cells in vitro using a feeder-free basement membrane substratum. PLoS ONE *6*, e24228.

Shyh-Chang, N., Locasale, J.W., Lyssiotis, C.A., Zheng, Y., Teo, R.Y., Ratanasirintrawoot, S., Zhang, J., Onder, T., Unternaehrer, J.J., Zhu, H., et al. (2013). Influence of threonine metabolism on S-adenosylmethionine and histone methylation. Science *339*, 222–226.

Suemori, H., Yasuchika, K., Hasegawa, K., Fujioka, T., Tsuneyoshi, N., and Nakatsuji, N. (2006). Efficient establishment of human embryonic stem cell lines and long-term maintenance with stable karyotype by enzymatic bulk passage. Biochem. Biophys. Res. Commun. *345*, 926–932.

Sufrin, J.R., Coulter, A.W., and Talalay, P. (1979). Structural and conformational analogues of L-methionine as inhibitors of the enzymatic synthesis of S-adenosyl-L-methionine. IV. Further mono-, bi- and tricyclic amino acids. Mol. Pharmacol. *15*, 661–677.

Takahashi, K., Tanabe, K., Ohnuki, M., Narita, M., Ichisaka, T., Tomoda, K., and Yamanaka, S. (2007). Induction of pluripotent stem cells from adult human fibroblasts by defined factors. Cell *131*, 861–872.

Takubo, K., Nagamatsu, G., Kobayashi, C.I., Nakamura-Ishizu, A., Kobayashi, H., Ikeda, E., Goda, N., Rahimi, Y., Johnson, R.S., Soga, T., et al. (2013). Regulation of glycolysis by Pdk functions as a metabolic checkpoint for cell cycle quiescence in hematopoietic stem cells. Cell Stem Cell *12*, 49–61.

Tohyama, S., Hattori, F., Sano, M., Hishiki, T., Nagahata, Y., Matsuura, T., Hashimoto, H., Suzuki, T., Yamashita, H., Satoh, Y., et al. (2013). Distinct metabolic flow enables large-scale purification of mouse and human pluripotent stem cell-derived cardiomyocytes. Cell Stem Cell *12*, 127–137.

Umeda, K., Suzuki, K., Yamazoe, T., Shiraki, N., Higuchi, Y., Tokieda, K., Kume, K., Mitani, K., and Kume, S. (2013). Albumin gene targeting in human embryonic stem cells and induced pluripotent stem cells with helper-dependent adenoviral vector to monitor hepatic differentiation. Stem Cell Res. (Amst.) *10*, 179–194.

Wang, J., Alexander, P., Wu, L., Hammer, R., Cleaver, O., and McKnight, S.L. (2009). Dependence of mouse embryonic stem cells on threonine catabolism. Science *325*, 435–439.

Wellen, K.E., and Thompson, C.B. (2012). A two-way street: reciprocal regulation of metabolism and signalling. Nat. Rev. Mol. Cell Biol. *13*, 270–276.

Zhang, X., Neganova, I., Przyborski, S., Yang, C., Cooke, M., Atkinson, S.P., Anyfantis, G., Fenyk, S., Keith, W.N., Hoare, S.F., et al. (2009). A role for NANOG in G1 to S transition in human embryonic stem cells through direct binding of CDK6 and CDC25A. J. Cell Biol. *184*, 67–82.

FEBS Letters 589 (2015) 849–856

FEBS Letters

journal homepage: www.FEBSLetters.org

CHF5074 (CSP-1103) stabilizes human transthyretin in mice humanized at the transthyretin and retinol-binding protein loci☆

Yanshuang Mu[b,c,1], Shoude Jin[d,1], Jingling Shen[a], Aki Sugano[e], Yutaka Takaoka[e], Lixia Qiang[b], Bruno P. Imbimbo[f], Ken-ichi Yamamura[b], Zhenghua Li[a,b,*]

[a] Department of Histology and Embryology, Harbin Medical University, Harbin, China
[b] Institute of Resource Development and Analysis, Kumamoto University, Kumamoto, Japan
[c] College of Life Sciences, Northeast Agriculture University, Harbin, China
[d] Division of Respiratory Disease, The Fourth Affiliated Hospital of Harbin Medical University, Harbin, China
[e] Division of Medical Informatics and Bioinformatics, Kobe University Hospital, Kobe, Japan
[f] Research and Development, Chiesi Farmaceutici, Parma, Italy

ARTICLE INFO

Article history:
Received 9 December 2014
Revised 12 February 2015
Accepted 17 February 2015
Available online 26 February 2015

Edited by Jesus Avila

Keywords:
CHF5074 (CSP-1103)
Familial amyloidotic polyneuropathy
Misfolding
Retinol binding protein
Transthyretin

ABSTRACT

Familial amyloidotic polyneuropathy is one type of protein misfolding disease. Transthyretin (TTR) tetramer dissociation is the limiting step for amyloid fibril formation. CHF5074 (CSP-1103) stabilizes TTR tetramer in vitro by binding to the T4 binding site. Here, we used three strains of double humanized mice ($mTtr^{hTTRVal30/hTTRVal30}$, $mTtr^{hTTRVal30/hTTRMet30}$, and $mTtr^{hTTRMet30/hTTRMet30}$) to assess whether CHF5074 stabilizes TTR tetramers in vivo. Treatment of mice with CHF5074 increased serum TTR levels by stabilizing TTR tetramers. Although the binding affinities of CHF5074 and diflunisal with TTRMet30 were similar, CHF5074 bound TTRVal30 more strongly than did diflunisal, suggesting the potent TTR-stabilizing activity of CHF5074.

1. Introduction

Familial amyloidotic polyneuropathy is an autosomal dominant disorder caused by a point mutation in the transthyretin (TTR) gene. TTR is a 127-amino acid, 55-kDa homotetrameric protein that circulates as a tetramer composed of four identical, non-covalently associated subunits [1,2]. TTR serves as a transport molecule for thyroxine (T4) and retinol binding protein (RBP). The process of TTR amyloidogenesis involves rate-limiting dissociation of TTR tetramer, followed by partial unfolding of monomers to yield non-fibrillar aggregates, protofibrils, and mature amyloid fibrils [3–5]. Structural studies of the TTR tetramer have disclosed several negatively cooperative compounds that bind to the T4 hormone pocket of TTR, consequently stabilizing the soluble form of TTR and inhibiting fibril formation [6–9].

CHF5074 (CSP-1103) [1-(3′,4′-dichloro-2-fluoro[1,1′-biphenyl]-4-yl)-cyclopropane carboxylic acid] is a non-steroidal anti-inflammatory derivative that lacks cyclooxygenase inhibitory activity. CHF5074 stimulates the phagocytic activity of microglia [10] and inhibits β-amyloid plaque deposition in the brains of various transgenic mouse models of Alzheimer disease [11–15]. X-ray analysis of the TTR crystal structure recently revealed that CHF5074 binds to the T4 sites of TTR tetramer and prevents acidic pH-induced TTR dissociation in vitro [16].

To assess the in vivo efficacy of drug candidates, animal models that reproduce the pathology of human TTR-mediated familial amyloidosis are required. By using a Cre-mediated recombination system, we previously produced humanized mice carrying either human normal (Val30) or mutant (Met30) TTR cDNA at the mouse *Ttr* locus [17]. By using the same strategy, we also created a humanized mouse carrying the human RBP gene at the mouse Rbp locus (manuscript, submitted). We then crossed these two lines to generate mice humanized at both the *Ttr* locus and the

Abbreviations: CHF5074, [1-(3′,4′-dichloro-2-fluoro[1,1′-biphenyl]-4-yl)-cyclopropane carboxylic acid]; RBP, retinol binding protein; T4, thyroxin; TTR, transthyretin

☆ Author contributions: Z.L. and K.Y. conceived and designed the experiments; Y.M., S.J., J.S., L.Q. and Z.L. performed the experiments; A.S. and Y.T. analyzed the data; and Z.L., B.P.I. and K.Y. wrote the paper.

* Corresponding author at: Department of Histology and Embryology, Harbin Medical University, 194 Xuefu Road, Nangang District, Harbin 150081, China. Fax: +86 451 86674518, +81 96 373 6596.
E-mail address: liseika@kumamoto-u.ac.jp (Z. Li).

[1] These authors contributed equally.

http://dx.doi.org/10.1016/j.febslet.2015.02.020
0014-5793/

Rbp locus. To test the stabilizing activity of CHF5074 in vivo, it would be better to humanize not only TTR but its binding molecules to mimic the physiological condition of human serum further. We therefore crossed these two lines to generate mice humanized at both the Ttr locus and the Rbp locus in which human TTR binds with human RBP4.

Here, we examined the short-term effect of oral CHF5074 administration on hTTR tetramer stabilization in mice humanized for both TTR and RBP. The data showed that CHF5074 stabilized TTR tetramers to increase serum levels of hVal30 and hMet30, suggesting that CHF5074 is a viable candidate inhibitor of TTR amyloid.

2. Materials and methods

2.1. Animals and CHF5074 treatment

All animal experiments were performed in accordance with the recommendations in the *Guide for the Care and Use of Laboratory Animals* of the US National Institutes of Health. The mouse lines carrying either normal human TTR (hVal30) ($mTtr^{hTTRVal30/hTTRVal30}$) or mutant human TTR (hMet30) ($mTtr^{hTTRMet30/hTTRMet30}$) at the mouse *Ttr* locus (humanized TTR mice) have been described previously [17]. Mouse lines with human *Rbp4* at the mouse *Rbp4* locus ($mRbp4^{hRBP4}$) (humanized Rbp4 mice) were produced in a similar way to the hTTR mice (manuscript in submission).

We used three mouse strains, $mTtr^{hTTRVal30/hTTRVal30}$:$mRbp4^{hRBP4/hRBP4}$ (hVal30:hRBP4), $mTtr^{hTTRVal30/hTTRMet30}$:$mRbp4^{hRBP4/hRBP4}$ (hVal30/Met30:hRBP4), and $mTtr^{hTTRMet30/hTTRMet30}$:$mRbp4^{hRBP4/hRBP4}$ (hMet30:hRBP4). Beginning at 13 weeks of age, mice were fed a CHF5074-containing diet (375 ppm, corresponding to about 60 μγ/kg/day). To analyze hepatic mRNA expression of the TTR or hRBP4 gene, liver samples for RNA isolation were obtained after 0, 3, 7, and 14 days of CHF5074 feeding. To evaluate serum hTTR and hRBP4 levels, blood samples were collected from the retro-orbital sinus at 0, 3, 7, 14, 21 and 28 days. To assess the stability of hTTR, blood samples were obtained at 0, 3, 7 and 14 days.

2.2. Semi-quantitative RT-PCR analyses

Semi-quantitative RT-PCR analyses were performed as described previously [18]. To assess hTTR mRNA expression, we used the primers mhTTR-F1 (sense, 5′-GTCCTCTGATGGTCAAAG T-3′) and mhTTR-R2 (anti-sense, 5′-GAGTCGTTGGCTGTGAA-3′). For evaluation of hRBP4 mRNA, we used mhRBP4-F (sense, 5′-GAG TCA AGG AGA ACT TCG AC-3′) and mhRBP4-e4R (antisense, 5′-CAG TAC TTC ATC TTG AAC TTG G-3′). The primers used for detection of mRNA from the housekeeping gene *Hprt* were 5′-CAC AGG ACT AGA ACA CCT GC-3′ (sense) and 5′-GCT GGT GAA AAG GAC CTC T-3′ (antisense). Amplified PCR products were separated by 1.5% agarose gel electrophoresis and visualized by ethidium bromide staining.

2.3. Serum hTTR and hRBP4 levels

Commercial ELISA kits were used according to the manufacturers' instructions to determine serum concentrations of hTTR (KA0495, Abnova, Taipei, China) and hRBP4 (AG-45A-0035, AdipoGen, San Diego, CA, USA).

2.4. Evaluation of serum TTR tetramer stability against acid- or urea-mediated denaturation

Dissociation of TTR tetramers and unfolding of monomers are accelerated under acidic or high-urea conditions [3,4]. Therefore, we used acid- or urea-mediated denaturation to discern the stability of hTTR in the sera of these mice. The extent of denaturation of hTTR from mice fed either the CHF5074-containing or control diet can be assessed by evaluating how much folded tetramer remains.

Blood samples were processed according to methods described elsewhere [19,20]. Acid- or urea-treated samples subsequently underwent gradient (10–20%) denaturing polyacrylamide gel electrophoresis. Separated proteins were transferred onto polyvinylidene difluoride membranes (BioRad Laboratories, Hercules, CA, USA) and then reacted with a polyclonal anti-TTR primary antibody (1:500) (Sigma, St. Louis, MO, USA) and a horseradish-peroxidase–conjugated secondary antibody (1:2500) (GE Healthcare, Dornstadt, Germany). The blotted proteins were quantified by using ECL Western Blotting Detection Reagents (GE Healthcare).

2.5. Statistical analysis of serum hTTR stability

To quantify the stability of serum hTTR tetramers, the densities of all TTR bands were quantified by using ImageJ software (version 1.48v, http://rsb.info.nih.gov/ij/docs/index.html). hTTR stability was evaluated according to the percentage of tetrameric hTTR or folded TTR (tetramers, trimers, and dimers) remaining by using the following formulas:

$$\%\ \text{tetramer at time } t = 100\% \times (\text{tetramer density at pH 4.0, time } t) / (\text{tetramer density at pH7, time 0})$$

$$\%\ \text{tetramer at time } t = 100\% \times (\text{tetramer density at 6 M urea, time } t) / (\text{tetramer density at 0 M urea, time 0})$$

$$\%\ \text{folded TTR at time } t = 100\% \times (\text{folded TTR at pH 7.0, time } t) / (\text{folded TTR at pH 7.0, time 0})$$

Results are expressed as means ± standard error of the mean. The percentages of tetrameric TTR of different hTTR variants from mice with and without drug treatment were compared by using *t*-tests. Differences were considered statistically significant at $P < 0.05$.

2.6. 3-D structures of the TTR tetramer

The 3-D structure of wild-type human TTR tetrameric complex was downloaded from the Protein Data Bank (PDB ID: 1rlb). The 3-D structure of the hMet30 mutant was constructed by creating a Val30Met substitution in wild-type hTTR. Then we subjected the structure of the hMet30 tetramer to molecular mechanics calculations by using MOE software (version 2011.10, Chemical Computing Group, Montreal, Quebec, Canada) with the AMBER99 force field and the generalized Born solvation model until the root mean square gradient was 0.01 kcal mol^{-1} $Å^{-1}$. This was followed by 5-ns molecular dynamics simulations at 310 K.

2.7. Docking simulation of TTR and CHF5074

We performed 100 docking runs of CHF5074 and hVal30 or hMet30 tetramers by using MOE Dock (Chemical Computing Group). The 3-D structure of CHF5074 was downloaded from ChemIDPlus (registry number, 749269-83-8). The docking sites of CHF5074 were determined as the T4 binding site (PDB ID: 1ict). Because the hTTR tetramer has two T4 binding sites, one or two ligand molecules were bound to each TTR tetramer. The complex comprising hVal30 or hMet30 tetramer and one or two molecules of CHF5074 that had the lowest S score was selected and subjected to molecular mechanics calculation by using MOE software with the OPLS-AA force field and the generalized Born solvation model

until the root mean square gradient was 0.01 kcal mol^{-1} $Å^{-1}$, followed by 5-ns molecular dynamics simulations at 310 K. The interaction energies between CHF5074 and the four hTTR subunits were calculated by using the potential energy function in the MOE software.

3. Results

Oral CHF5074 was well tolerated by all mice; no obvious side effects were observed during or after the study, according to body weight and the results of physical examination, blood biochemistry and hematology analyses.

3.1. Effects of CHF5074 on serum hTTR levels

Before CHF5074 treatment, the serum level of hVal30 (wild-type) in hVal30:hRBP4 mice was 4.04 ± 0.15 μg/mL, and that of hMet30 (mutant) in hMet30:hRBP4 mice was 0.56 ± 0.14 μg/mL. Given that hepatic TTR mRNA expression was similar in hVal30:hRBP4 and hMet30:hRBP4 mice, the low serum level of hMet30 likely was due to the instability of hMet30 tetramers in the serum. In hVal30:hRBP4 mice, the serum level of hVal30 was increased 3 days after the start of the CHF5074 diet compared with pretreatment concentrations and remained at similar levels (5.10–6.12 μg/mL) thereafter. The maximal level of serum hVal30 was about 1.5 times that before treatment (Fig. 1A). To assess whether the increase in serum TTR concentrations was due to an increase in the amount of hVal30 tetramer, we used Western blot analysis to determine the level of tetramer. The amount of hVal30 tetramer in the serum was increased 3 days after the start of the CHF5074 diet and remained at similar levels (1.46–1.55 times the pretreatment level) thereafter (Fig. 1B).

In hMet30:hRBP4 mice, the serum concentration of hTTR was increased 3 days after the start of the CHF5074 diet and remained at similar levels (1.73–2.68 μg/mL) thereafter. The maximal level of serum hMet30 was about 5 times that before treatment but was only 30–40% that of hVal30 in Val30:hRBP4 mice (Fig. 1B). As seen for hVal30 tetramer, this increase was due to an increase in hMet30 tetramers. The amount of hMet30 tetramer in the serum was increased to 2.03, 5.77, and 5.63 times the pretreatment level at 3, 7, and 14 days, respectively, after the start of the CHF5074 diet (Fig. 1D). Furthermore, levels of trimers and dimers were increased in addition to those of tetramers (Fig. 1B and D), suggesting that CHF5074 can bind to TTR trimers and dimers. These results suggest that the increased levels of serum hVal30 and hMet30 were due to stabilization of tetramers after the binding of CHF5074 and that the

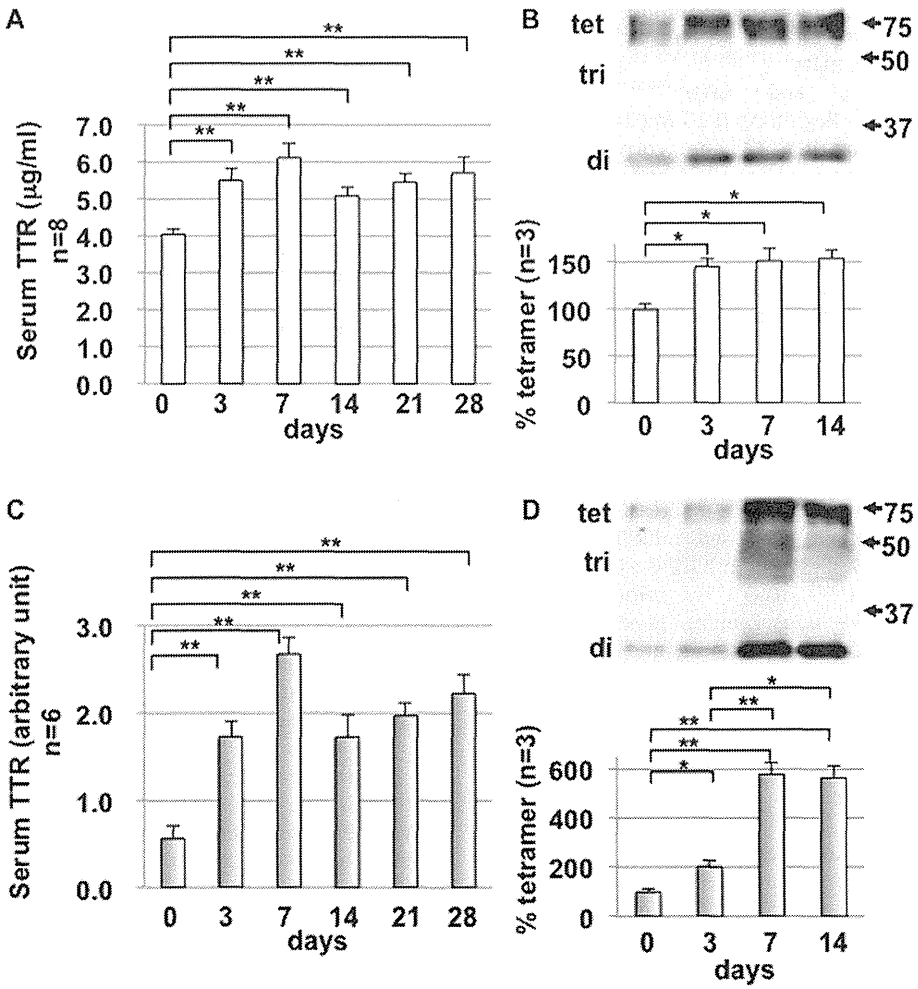

Fig. 1. Effect of CHF5074 on serum concentrations of TTR tetramers. (A) Serum hTTR levels in hVal30:hRBP4 mice. Serum hVal30 levels increased approximately 1.4 times on average after CHF5074 treatment. (B) Serum Val30 tetramer levels in hVal30:hRBP4 mice. Serum hVal30 levels increased approximately 1.5 times on average after CHF5074 treatment. (C) Serum hTTR levels in hMet30:hRBP4 mice. Serum hMet30 levels increased about 3.7 times on average after CHF5074 treatment. (D) Serum Met30 tetramer levels in hMet30:hRBP4 mice. Serum hMet30 levels increased approximately 2.0, 5.8, and 5.6 times at 3, 7, and 14 days, respectively, after the start of the CHF5074 diet. $^{*}P < 0.05$; $^{**}P < 0.01$.

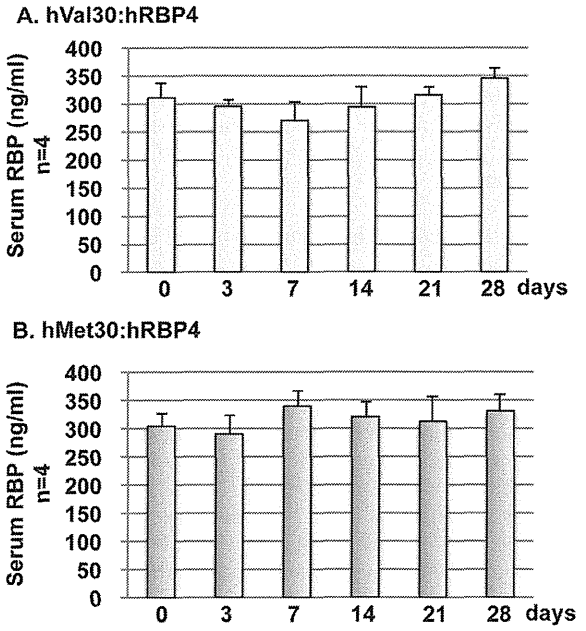

Fig. 2. Effect of CHF5074 on serum concentrations of RBP4. (A) Serum hRBP4 levels in hVal30:hRBP4 mice. Serum hRBP4 levels before and after CHF5074 treatment did not differ. (B) Serum hRBP4 levels in hMet30:hRBP4 mice. Serum hRBP4 levels before and after CHF5074 treatment did not differ. $^{**}P < 0.01$.

stabilization effect of CHF5074 was more intense in hMet30:RBP4 than in hVal30:hRBP4 mice.

3.2. Effects of CHF5074 on serum hRBP4 levels

Serum levels of hRBP4 did not change in either hVal30:hRBP4 or hMet30:hRBP4 mice after provision of the CHF5074-containing diet (Fig. 2).

3.3. Effects of CHF5074 on hepatic expression of hTTR and hRBP4 mRNAs

To analyze whether the increased serum TTR concentrations after CHF5074 supplementation were due to increased TTR transcription, we examined the levels of hTTR mRNA in liver. Quantities of hVal30 or hMet30 mRNA in hVal30:hRBP4 or hMet30:hRBP4 mice did not change after provision of the CHF5074 diet (Fig. 3). These results suggested that CHF5074 did not affect hepatic hTTR mRNA expression. In addition, the amounts of hRBP4 in hVal30:hRBP4 and hMet30:hRBP4 mice did not change after provision of the CHF5074 diet (Fig. 3).

3.4. CHF5074 stabilizes serum hTTR under acidic conditions

We analyzed the CHF5074-associated kinetic stabilization of hTTR under denaturation stress. As described before, the effect of a diet containing CHF5074 for 28 days on the extent of denaturation of hTTR tetramer can be assessed by evaluating how much tetramer or folded TTR (tetramers, trimers, and dimers) remains.

The denaturation of hTTR tetramers under low pH conditions at 37 °C was monitored by Western blot. First, the stability of hVal30 homotetramers from mice given or not given dietary CHF5074 was assessed after exposing the serum samples to various pH (3.6–7.0) conditions for 3 days. The percentage of folded TTR (hVal30) was clearly higher in the presence of CHF5074 than in its absence at every pH condition tested (Fig. 4A). Because the folded TTR was dissociated almost completely at pH 4.0 in the absence of CHF5074, we used this pH condition in the following experiments.

The percentages of native hTTR tetramer (means ± standard error) from hVal30:hRBP4 and hVal30/hMet30:hRBP4 mice without CHF5074 treatment were lower than those from mice with CHF5074 treatment after denaturation stress at pH 4.0 for 24, 48, or 72 h (Fig. 4B). For hMet30:hRBP4 mice, the percentage of native tetramer in the absence of CHF5074 was lower than that with

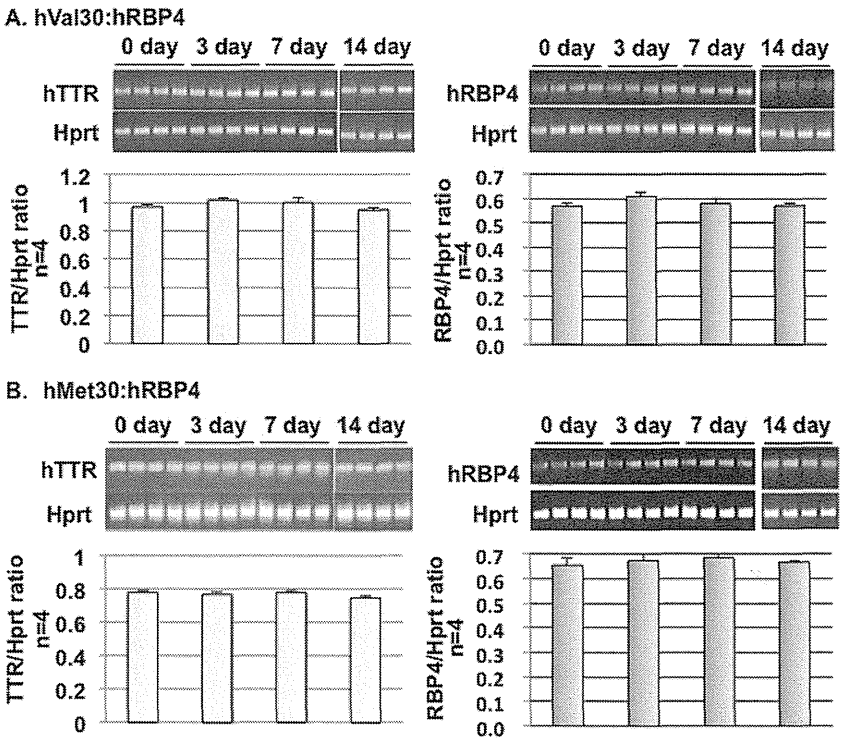

Fig. 3. Effect of CHF5074 on hepatic levels of hTTR and hRBP4 mRNA. (A) RT-PCR of mRNA isolated from hVal30:hRBP4 mice. (B) RT-PCR of mRNA isolated from hMet30:hRBP4 mice. Total RNA isolated from liver samples was harvested on day 0 and on days 3, 7, and 14 after initiation of the CHF5074-containing diet and was subjected to semi-quantitative RT-PCR analysis. hTTR and hRBP4 mRNA expression levels did not differ between any time points.

CHF5074 treatment, but only after 12 h at pH 4 (Fig. 4B). These results suggest that CHF5074 effectively stabilized hVal30 homotetramers and hVal30–hMet30 heterotetramers but that hMet30 homotetramers were more unstable than were the other tetramers, even in the presence of CHF5074. Therefore, the denaturation stress associated with pH 4.0 conditions may be too strong for hMet30 homotetramers to withstand, even in the presence of CHF5074.

3.5. CHF5074 stabilizes serum hTTR under urea denaturation conditions

To determine the optimal concentration of urea at which to test the stability of hTTR tetramers, serum samples from hVal30:hRBP4 mice before and after CHF5074 feeding were incubated in various concentrations of urea (0–10 M) for 3 days. The folded TTR (hVal30) was clearly more stable in the presence of CHF5074 than in its absence at every urea concentration tested (Fig. 5A). When 6 M urea was used, the percentage of folded TTR after CHF5074 feeding was clearly higher than that in the absence of CHF5074; we therefore used that denaturation condition in the following experiments.

After denaturation stress with 6 M urea, the percentage of native hTTR tetramer from hVal30:hRBP4 mice fed the control diet was lower than that in mice fed the CHF5074 diet at the 24-, 48-, and 72-h time points (Fig. 5B). The percentage of native hTTR tetramer in hVal30/hMet30:hRBP4 mice was lower in the absence of CHF5074 than with CHF5074 after urea denaturation for 12, 24, 48, or 72 h (Fig. 5B). In hMet30:hRBP4 mice, the percentage of native hTTR tetramer without CHF5074 was lower than that after CHF5074 at the 24-, 48-, and 72-h time points for urea exposure (Fig. 5B). These results are similar in pattern to those after exposure to acidic pH, again suggesting that CHF5074 effectively stabilizes TTR tetramers.

3.6. Computational studies of binding affinity of CHF5074 with TTR tetramer

Diflunisal is a well-characterized inhibitor of fibrillogenesis [21]. Although the mode of binding to the T4 sites of TTR differs between CHF5074 and diflunisal, these two fibrillogenesis inhibitors exhibit similar stabilizing effects on TTR structure [16]. We therefore used computational docking simulation analysis to study the binding affinity between TTR and CHF5074 or diflunisal.

The structures of T4 and CHF5074 (Fig. 6A) are similar, as are their modes of binding to TTR (Fig. 6B). The binding affinity of CHF5074 for hMet30 was similar to that of diflunisal, whereas CHF5074 bound hVal30 with much greater affinity than did diflunisal (Table 1).

4. Discussion

We demonstrated that CHF5074 stabilized both normal and mutant TTR tetramers against denaturing stresses due to both acid

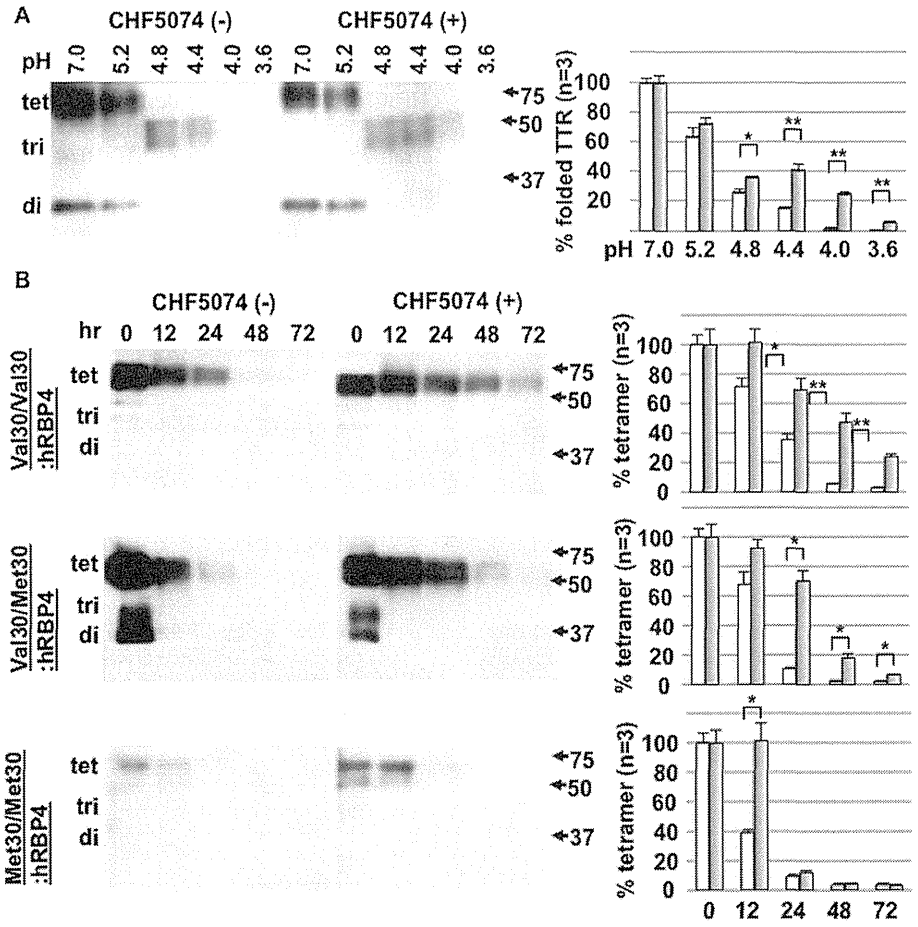

Fig. 4. Resistance to acid-mediated denaturation of serum hTTR from mice fed the CHF5074-containing or control diet. (A) Serum hTTR with and without CHF5074 after denaturation (72 h) under various pH conditions. The folded TTR dissociated almost completely at pH 4.0 in the absence of CHF5074. (B) Time course of acid-induced denaturation (pH 4.0) of serum hTTR with or without CHF5074. Three types of tetramers (hVal30 homotetramers, hVal30–hMet30 heterotetramers, and hMet30 homotetramers) were stabilized after CHF5074 supplementation of mice. $^{*}P < 0.05$; $^{**}P < 0.01$.

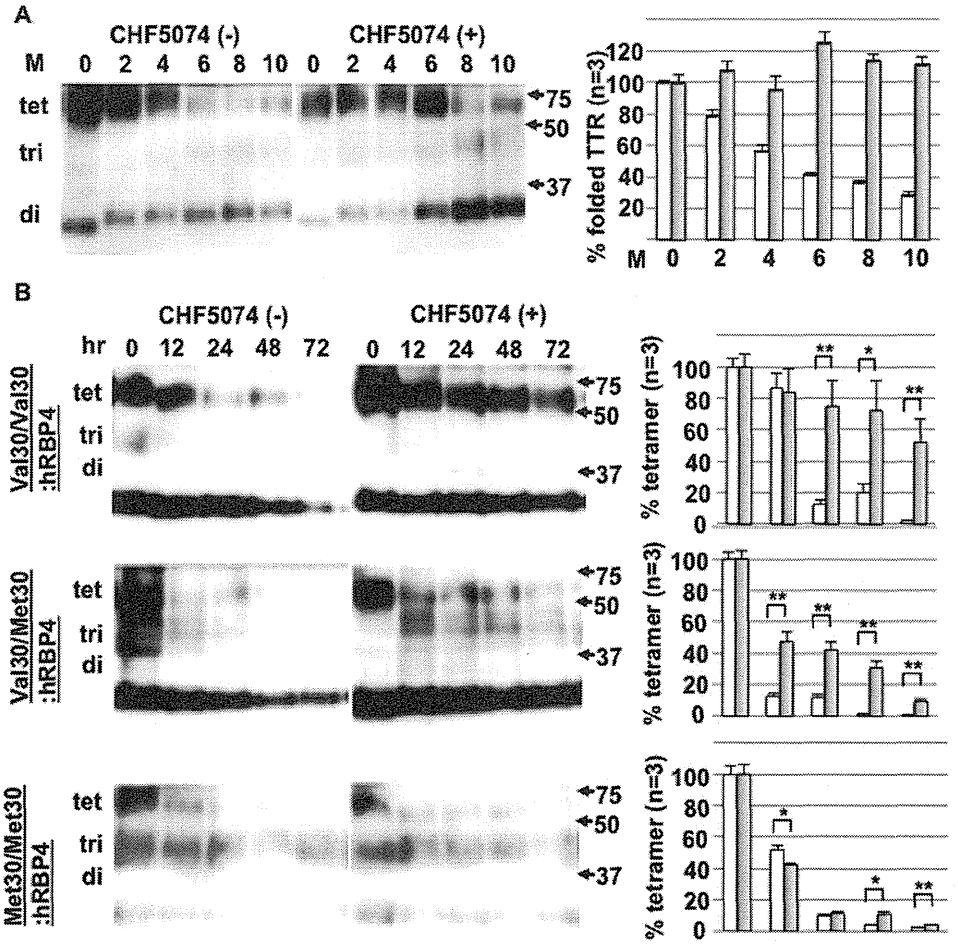

Fig. 5. Resistance to urea-mediated denaturation of serum hTTR from mice fed the CHF5074-containing or control diet. (A) Time course of urea-induced denaturation (6 M) of serum hTTR with or without CHF5074. Serum hTTR with and without CHF5074 after denaturation (72 h) at various concentrations of urea. At 6 M urea, the percentage of folded TTR after CHF5074 feeding was clearly higher than that in the absence of CHF5074. (B) Quantitative analysis of serum hTTR stability. Two types of tetramers (hVal30 homotetramers and hVal30–hMet30 heterotetramers) were stabilized after CHF5074 supplementation of mice. $^{*}P < 0.05$; $^{**}P < 0.01$.

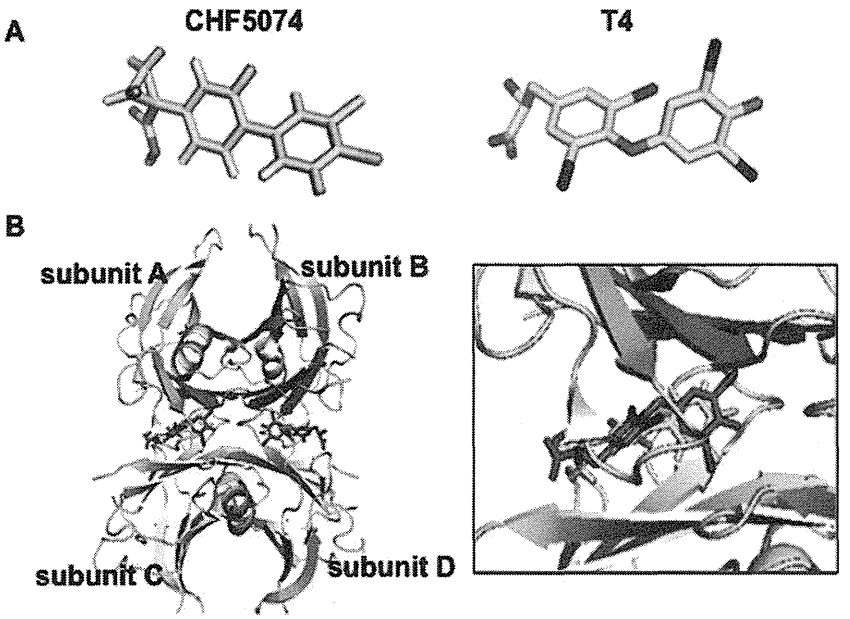

Fig. 6. Computational studies of binding affinity of CHF5074 for TTR tetramer (A) Structural diagram of TTR ligands. Carbon, green; hydrogen, white; nitrogen, blue; iodide, purple; oxygen, red; chloride, gray; fluoride, light blue. B. Proposed structure of hTTR in complex with CHF5074 at pH 7.0. The ribbon diagram of tetrameric TTR with bound ligand within the two T4 binding pockets, at the weak dimer–dimer interface, is shown. The close-up view depicts TTR within a single binding site. Green, CHF5074; purple, T4.

Table 1
Computational studies of binding affinity.

ZDOCK score (kcal/molecule)		CHF5074			Diflunisal		
		One molecule binding		Two molecule binding	One molecule binding		Two molecule binding
		Binding between A and C	Binding between B and D		Binding between A and C	Binding between B and D	
TTRVal30	A	−24.0		−16.7	−18.5		−12.1
	B		−14.0	−23.6		−10.9	−4.0
	C	−14.3		−26.1	−9.3		−19.8
	D		−25.1	−19.7		−7.9	−10.0
	Total	−38.3	−39.0	−86.1	−27.8	−18.8	−45.9
TTR Met30	A	−24.6		−26.1	−18.5		−13.0
	B		−14.6	−13.6		−15.5	−20.1
	C	−14.8		−8.1	−9.4		−15.6
	D		−14.2	−21.5		−6.6	−17.7
	Total	−39.4	−28.8	−69.3	−27.9	−22.1	−66.4

Potential energy was expressed as kcal/mol. There was a significant difference in the potential energy between TTRVal30-CHF5074 and TTRVal30-diflunisal.

and urea, thereby increasing the serum TTR levels of mice fed a CHF5074-containing diet. These data are consistent with the results we obtained from computational studies of binding affinity.hVal30 (that is, wild-type) levels in the sera of our humanized mice were about 1/100 those in humans (200–400 μg/mL). As described previously, the serum levels of hTTR homotetramers were much lower than expected because of the instability of hTTR tetramers in mice [17]. Similarly, serum hRBP4 levels in our humanized mice were about 1/100 those in humans (20–60 μg/mL). Consequently, the hTTR:hRBP4 ratio in our humanized mice was about 10:1, consistent with that in humans. As expected, the serum levels of hMet30 TTR tetramers in hMet30:hRBP4 mice were about 7 times lower than those of hVal30 TTR tetramers in hVal30:hRBP4 mice, even though hepatic mRNA expression levels were similar in the two strains. These findings clearly suggest that hMet30 tetramers were much more unstable than were hVal30 tetramers in serum. Therefore, our double-humanized mice may be an effective model for evaluating the stabilizing effects of small molecules for hTTR tetramers.

Numerous small molecules have been discovered to impose kinetic stabilization on the TTR native state [22–31]. Many of these kinetic stabilizers of TTR are derivatives of non-steroidal anti-inflammatory drugs with anti-cyclooxygenase activity. Accordingly, these inhibitors are associated with various adverse side effects [32–35]. Conversely, the anti-COX activity of flurbiprofen was removed by modification at the alpha position, leading to the production of CHF5074 [36]. Treatment with CHF5074 (375 ppm in the diet) attenuated brain β-amyloid pathology and learning–memory deficits in a transgenic mouse model of Alzheimer disease [13–15]. In accordance with these results, serum hVal30 and hMet30 levels were increased about 1.5 times in hVal30:hRBP4 or approximately 5 times in hMet30:hRBP4 mice after treatment with CHF5074 (375 ppm in the diet). These increases were due to the CHF5074-associated stabilization of TTR tetramers, as demonstrated by the data from the pH and urea denaturation assays.

Previous analysis of the crystal structures of CHF5074 and TTR tetramers revealed that CHF5074 binds to the T4-binding sites of TTR and inhibits TTR amyloidosis in vitro [16]. Our computer simulation analysis confirmed that CHF5074 binds to the T4 sites of TTR tetramer. Interestingly, the binding affinity of CHF5074 for hVal30 was much higher than that of diflunisal, but CHF5074 and diflunisal had similar affinities for hMet30. Given that most patients with familial amyloidotic neuropathy are heterozygous for the condition, having TTR heterotetramer composed of both hVal30 and hMet30 monomers, the stabilizing activity of CHF5074 may be more potent than that of diflunisal in clinical applications.

Liver transplantation does not ameliorate deposition of TTR in the eye and central nervous system [37], owing to TTR synthesis by the retinal pigment epithelium and choroid plexus. Because CHF5074 efficiently crosses the blood–brain barrier [12,13,15], this compound may be effective against amyloidosis in the eye and central nervous system.

In conclusion, CHF5074 is a promising candidate for the treatment of familial amyloid polyneuropathy owing to its stabilization of hTTR tetramers and its lack of toxic effects.

Conflict of interest statement

This study was partly funded by Chiesi Farmaceutici, Parma, Italy.

Acknowledgments

This work was supported by Grants-in-Aid for Scientific Research (C) from the Japan Society for the Promotion of Science (to Z.L.) and by Grants-in-Aid for Scientific Research (S) from the Japan Society for the Promotion of Science and CREST (JST) (to K.Y.).

References

[1] Schreiber, G. (2002) The evolution of transthyretin synthesis in the choroid plexus. Clin. Chem. Lab. Med. 40, 1200–1210.
[2] Vranckx, R., Savu, L., Maya, M. and Nunez, E.A. (1990) Characterization of a major development-regulated serum thyroxine-binding globulin in the euthyroid mouse. Biochem. J. 271, 373–379.
[3] Colon, W. and Kelly, J.W. (1992) Partial denaturation of transthyretin is sufficient for amyloid fibril formation in vitro. Biochemistry 31, 8654–8660.
[4] Hammarstrom, P., Jiang, X., Hurshman, A.R., Powers, E.T. and Kelly, J.W. (2002) Sequence-dependent denaturation energetics: a major determinant in amyloid disease diversity. Proc. Natl. Acad. Sci. USA 99 (Suppl. 4), 16427–16432.
[5] Lai, Z., Colon, W. and Kelly, J.W. (1996) The acid-mediated denaturation pathway of transthyretin yields a conformational intermediate that can self-assemble into amyloid. Biochemistry 35, 6470–6482.
[6] Johnson, S.M., Wiseman, R.L., Sekijima, Y., Green, N.S., Adamski-Werner, S.L. and Kelly, J.W. (2005) Native state kinetic stabilization as a strategy to ameliorate protein misfolding diseases: a focus on the transthyretin amyloidosis. Acc. Chem. Res. 38, 911–921.
[7] Klabunde, T., Petrassi, H.M., Oza, V.B., Raman, P., Kelly, J.W. and Sacchettini, J.C. (2000) Rational design of potent human transthyretin amyloid disease inhibitors. Nat. Struct. Biol. 7, 312–321.
[8] Miroy, G.J., Lai, Z., Lashuel, H.A., Peterson, S.A., Strang, C. and Kelly, J.W. (1996) Inhibiting transthyretin amyloid fibril formation via protein stabilization. Proc. Natl. Acad. Sci. USA 93, 15051–15056.
[9] Sekijima, Y., Kelly, J.W. and Ikeda, S. (2008) Pathogenesis of and therapeutic strategies to ameliorate the transthyretin amyloidoses. Curr. Pharm. Des. 14, 3219–3230.
[10] Porrini, V., Lanzillotta, A., Branca, C., Benarese, M., Parrella, E., Lorenzini, L., Calzà, L., Flaibani, R., Spano, P., Imbimbo, B. P. & Pizzi, M. (in press) CHF5074

(CSP-1103) induces microglia alternative activation in plaque-free Tg2576 mice and primary glial cultures exposed to β-amyloid, *Neurosci.* in press.
[11] Balducci, C., Mehdawy, B., Mare, L., Giuliani, A., Lorenzini, L., Sivilia, S., Giardino, L., Calza, L., Lanzillotta, A., Sarnico, I., Pizzi, M., Usiello, A., Viscomi, A.R., Ottonello, S., Villetti, G., Imbimbo, B.P., Nistico, G., Forloni, G. and Nistico, R. (2011) The gamma-secretase modulator CHF5074 restores memory and hippocampal synaptic plasticity in plaque-free Tg2576 mice. J. Alzheimers Dis. 24, 799–816.
[12] Imbimbo, B.P., Del Giudice, E., Cenacchi, V., Volta, R., Villetti, G., Facchinetti, F., Riccardi, B., Puccini, P., Moretto, N., Grassi, F., Ottonello, S. and Leon, A. (2007) In vitro and in vivo profiling of CHF5022 and CHF5074 Two beta-amyloid1-42 lowering agents. Pharmacol. Res. 55, 318–328.
[13] Imbimbo, B.P., Del Giudice, E., Colavito, D., D'Arrigo, A., Dalle Carbonare, M., Villetti, G., Facchinetti, F., Volta, R., Pietrini, V., Baroc, M.F., Serneels, L., De Strooper, B. and Leon, A. (2007) 1-(3′,4′-Dichloro-2-fluoro[1,1′-biphenyl]-4-yl)-cyclopropanecarboxylic acid (CHF5074), a novel gamma-secretase modulator, reduces brain beta-amyloid pathology in a transgenic mouse model of Alzheimer's disease without causing peripheral toxicity. J. Pharmacol. Exp. Ther. 323, 822–830.
[14] Imbimbo, B.P., Giardino, L., Sivilia, S., Giuliani, A., Gusciglio, M., Pietrini, V., Del Giudice, E., D'Arrigo, A., Leon, A., Villetti, G. and Calza, L. (2010) CHF5074, a novel gamma-secretase modulator, restores hippocampal neurogenesis potential and reverses contextual memory deficit in a transgenic mouse model of Alzheimer's disease. J. Alzheimers Dis. 20, 159–173.
[15] Imbimbo, B.P., Hutter-Paier, B., Villetti, G., Facchinetti, F., Cenacchi, V., Volta, R., Lanzillotta, A., Pizzi, M. and Windisch, M. (2009) CHF5074, a novel gamma-secretase modulator, attenuates brain beta-amyloid pathology and learning deficit in a mouse model of Alzheimer's disease. Br. J. Pharmacol. 156, 982–993.
[16] Zanotti, G., Cendron, L., Folli, C., Florio, P., Imbimbo, B.P. and Berni, R. (2013) Structural evidence for native state stabilization of a conformationally labile amyloidogenic transthyretin variant by fibrillogenesis inhibitors. FEBS Lett. 587, 2325–2331.
[17] Zhao, G., Li, Z., Araki, K., Haruna, K., Yamaguchi, K., Araki, M., Takeya, M., Ando, Y. and Yamamura, K.I. (2008) Inconsistency between hepatic expression and serum concentration of transthyretin in mice humanized at the transthyretin locus. Genes Cells 13, 1257–1268.
[18] Li, Z., Zhao, G., Shen, J., Araki, K., Haruna, K., Inoue, S., Wang, J. and Yamamura, K. (2011) Enhanced expression of human cDNA by phosphoglycerate kinase promoter-puromycin cassette in the mouse transthyretin locus. Transgenic Res. 20, 191–200.
[19] Sekijima, Y., Dendle, M.A. and Kelly, J.W. (2006) Orally administered diflunisal stabilizes transthyretin against dissociation required for amyloidogenesis. Amyloid 13, 236–249.
[20] Tojo, K., Sekijima, Y., Kelly, J.W. and Ikeda, S. (2006) Diflunisal stabilizes familial amyloid polyneuropathy-associated transthyretin variant tetramers in serum against dissociation required for amyloidogenesis. Neurosci. Res. 56, 441–449.
[21] Miller, S.R., Sekijima, Y. and Kelly, J.W. (2004) Native state stabilization by NSAIDs inhibits transthyretin amyloidogenesis from the most common familial disease variants. Lab. Invest. 84, 545–552.
[22] Adamski-Werner, S.L., Palaninathan, S.K., Sacchettini, J.C. and Kelly, J.W. (2004) Diflunisal analogues stabilize the native state of transthyretin. Potent inhibition of amyloidogenesis. J. Med. Chem. 47, 355–374.
[23] Baures, P.W., Oza, V.B., Peterson, S.A. and Kelly, J.W. (1999) Synthesis and evaluation of inhibitors of transthyretin amyloid formation based on the non-steroidal anti-inflammatory drug, flufenamic acid. Bioorg. Med. Chem. 7, 1339–1347.
[24] Bulawa, C.E., Connelly, S., Devit, M., Wang, L., Weigel, C., Fleming, J.A., Packman, J., Powers, E.T., Wiseman, R.L., Foss, T.R., Wilson, I.A., Kelly, J.W. and Labaudiniere, R. (2012) Tafamidis, a potent and selective transthyretin kinetic stabilizer that inhibits the amyloid cascade. Proc. Natl. Acad. Sci. USA 109, 9629–9634.
[25] Green, N.S., Palaninathan, S.K., Sacchettini, J.C. and Kelly, J.W. (2003) Synthesis and characterization of potent bivalent amyloidosis inhibitors that bind prior to transthyretin tetramerization. J. Am. Chem. Soc. 125, 13404–13414.
[26] Oza, V.B., Petrassi, H.M., Purkey, H.E. and Kelly, J.W. (1999) Synthesis and evaluation of anthranilic acid-based transthyretin amyloid fibril inhibitors. Bioorg. Med. Chem. Lett. 9, 1–6.
[27] Penchala, S.C., Connelly, S., Wang, Y., Park, M.S., Zhao, L., Baranczak, A., Rappley, I., Vogel, H., Liedtke, M., Witteles, R.M., Powers, E.T., Reixach, N., Chan, W.K., Wilson, I.A., Kelly, J.W., Graef, I.A. and Alhamadsheh, M.M. (2013) AG10 inhibits amyloidogenesis and cellular toxicity of the familial amyloid cardiomyopathy-associated V122I transthyretin. Proc. Natl. Acad. Sci. USA 110, 9992–9997.
[28] Peterson, S.A., Klabunde, T., Lashuel, H.A., Purkey, H., Sacchettini, J.C. and Kelly, J.W. (1998) Inhibiting transthyretin conformational changes that lead to amyloid fibril formation. Proc. Natl. Acad. Sci. USA 95, 12956–12960.
[29] Purkey, H.E., Palaninathan, S.K., Kent, K.C., Smith, C., Safe, S.H., Sacchettini, J.C. and Kelly, J.W. (2004) Hydroxylated polychlorinated biphenyls selectively bind transthyretin in blood and inhibit amyloidogenesis: rationalizing rodent PCB toxicity. Chem. Biol. 11, 1719–1728.
[30] Razavi, H., Palaninathan, S.K., Powers, E.T., Wiseman, R.L., Purkey, H.E., Mohamedmohaideen, N.N., Deechongkit, S., Chiang, K.P., Dendle, M.T., Sacchettini, J.C. and Kelly, J.W. (2003) Benzoxazoles as transthyretin amyloid fibril inhibitors: synthesis, evaluation, and mechanism of action. Angew. Chem. Int. Ed. Engl. 42, 2758–2761.
[31] Razavi, H., Powers, E.T., Purkey, H.E., Adamski-Werner, S.L., Chiang, K.P., Dendle, M.T. and Kelly, J.W. (2005) Design, synthesis, and evaluation of oxazole transthyretin amyloidogenesis inhibitors. Bioorg. Med. Chem. Lett. 15, 1075–1078.
[32] Epstein, M. (2002) Non-steroidal anti-inflammatory drugs and the continuum of renal dysfunction. J. Hypertens. 20, S17–S23.
[33] Kearney, P.M., Baigent, C., Godwin, J., Halls, H., Emberson, J.R. and Patrono, C. (2006) Do selective cyclo-oxygenase-2 inhibitors and traditional non-steroidal anti-inflammatory drugs increase the risk of atherothrombosis? Meta-analysis of randomised trials. Br. Med. J. 332, 1302–1308.
[34] Khan, M. and Fraser, A. (2012) Cox-2 inhibitors and the risk of cardiovascular thrombotic events. Irish Med. J. 105, 119–121.
[35] Mukherjee, D., Nissen, S.E. and Topol, E.J. (2001) Risk of cardiovascular events associated with selective COX-2 inhibitors. J. Am. Med. Assoc. 286, 954–959.
[36] Peretto, I., Radaelli, S., Parini, C., Zandi, M., Raveglia, L.F., Dondio, G., Fontanella, L., Misiano, P., Bigogno, C., Rizzi, A., Riccardi, B., Biscaioli, M., Marchetti, S., Puccini, P., Catinella, S., Rondelli, I., Cenacchi, V., Bolzoni, P.T., Caruso, P., Villetti, G., Facchinetti, F., Del Giudice, E., Moretto, N. and Imbimbo, B.P. (2005) Synthesis and biological activity of flurbiprofen analogues as selective inhibitors of beta-amyloid(1)(-)(42) secretion. J. Med. Chem. 48, 5705–5720.
[37] Ando, Y., Terazaki, H., Nakamura, M., Ando, E., Haraoka, K., Yamashita, T., Ueda, M., Okabe, H., Sasaki, Y., Tanihara, H., Uchino, M. and Inomata, Y. (2004) A different amyloid formation mechanism: de novo oculoleptomeningeal amyloid deposits after liver transplantation. Transplant 77, 345–349.

Exp. Anim. 63(1), 79–84, 2014

—Original—

Screening Methods to Identify TALEN-Mediated Knockout Mice

Yoshiko NAKAGAWA[1)], Takashi YAMAMOTO[2)], Ken-Ichi SUZUKI[2)], Kimi ARAKI[1)], Naoki TAKEDA[1)], Masaki OHMURAYA[1)], and Tetsushi SAKUMA[2)]

[1)]*Center for Animal Resources and Development, Kumamoto University, 2–2–1 Honjo, Kumamoto 860-0811, Japan*
[2)]*Department of Mathematical and Life Sciences, Graduate School of Science, Hiroshima University, 1–3–1 Kagamiyama, Higashi-Hiroshima, Hiroshima 739-8526, Japan*

Abstract: Genome editing with site-specific nucleases, such as zinc-finger nucleases or transcription activator-like effector nucleases (TALENs), and RNA-guided nucleases, such as the CRISPR/Cas (clustered regularly interspaced short palindromic repeats/CRISPR-associated) system, is becoming the new standard for targeted genome modification in various organisms. Application of these techniques to the manufacture of knockout mice would be greatly aided by simple and easy methods for genotyping of mutant and wild-type pups among litters. However, there are no detailed or comparative reports concerning the identification of mutant mice generated using genome editing technologies. Here, we genotyped TALEN-derived enhanced green fluorescent protein (*eGFP*) knockout mice using a combination of approaches, including fluorescence observation, heteroduplex mobility assay, restriction fragment length polymorphism analysis and DNA sequencing. The detection sensitivities for TALEN-induced mutations differed among these methods, and we therefore concluded that combinatorial testing is necessary for the screening and determination of mutant genotypes. Since the analytical methods tested can be carried out without specialized equipment, costly reagents and/or sophisticated protocols, our report should be of interest to a broad range of researchers who are considering the application of genome editing technologies in various organisms.
Key words: genome editing, knockout mouse, TALEN, targeted mutagenesis

Introduction

Transcription activator-like effector (TALE) nuclease (TALEN)-mediated gene knockout technology is now applicable to a wide variety of cells and organisms [5]. Each TALEN comprises a TALE domain that binds to a specified DNA sequence and a nuclease domain derived from the *FokI* restriction endonuclease. When a pair of TALENs designed for a specific genomic locus is introduced into embryos, a DNA double-strand break (DSB) occurs at the target site. DSBs are mainly repaired by error-prone non-homologous end-joining (NHEJ), resulting in randomly induced insertions and deletions that cause disruption of gene functions [7].

Conventionally, knockout mice have been created using an embryonic stem (ES) cell-mediated strategy based on spontaneous homologous recombination between genomic DNA and a targeting construct [2]. This method is time-consuming and requires several laborious processes, such as construction of a gene targeting vector, isolation of targeted ES cell clones, production of chimeras, test breeding for germline transmission and, in some cases, backcrossing to another inbred background. However, the use of TALENs for gene targeting

(Received 13 June 2013 / Accepted 12 August 2013)
Address corresponding: T. Sakuma, Department of Mathematical and Life Sciences, Graduate School of Science, Hiroshima University, 1–3–1 Kagamiyama, Higashi-Hiroshima, Hiroshima 739-8526, Japan

enables knockout mice to be produced in a short time because the TALEN mRNAs are simply injected into the embryos of any intended inbred strain. Recently, several groups reported that knockout mice and rats could be efficiently created by TALEN-mediated gene targeting [4, 6, 10, 14, 16]. The convenience of this technique means that TALEN-mediated gene knockout will become a major method for the production of genetically modified rodents in the near future. However, while ES cell-mediated chimeric mice can easily be determined by their coat color, with TALEN-mediated gene targeting it is difficult to distinguish genetically modified mice from wild-type pups unless a phenotype is apparent.

Here, we injected TALEN mRNAs targeting the enhanced green fluorescent protein (*eGFP*) gene into fertilized mouse eggs expressing eGFP ubiquitously under control of the *CAG* promoter (*pCAG*). Pups were analyzed by observation of green fluorescence, heteroduplex mobility assay (HMA), restriction fragment length polymorphism (RFLP) analysis and DNA sequencing to consolidate the method for detecting pups with TALEN-induced mutations.

Materials and Methods

TALEN plasmid construction and mRNA preparation

Synthesized TALE repeats were cloned into pBluescript SK and assembled using the Golden Gate cloning method [12]. The N- and C-terminal domains of TALE and the *Fok*I nuclease domain were taken from pTALEN_v2 (Addgene, Cambridge, MA, USA) [13]. The *eGFP* TALEN target sequence was described previously [11] and is indicated in Fig. 1. TALEN mRNAs were synthesized from plasmids linearized by *Sma*I digestion using an mMessage mMachine T7 Ultra Kit (Life Technologies, Carlsbad, CA, USA) and purified with an RNeasy Mini Kit (Qiagen, Hilden, Germany) following the manufacturers' instructions and as previously described [11].

pCAG-eGFP mouse embryos

The parental *pCAG-eGFP* mouse strain has been deposited in the Center for Animal Resources and Development (CARD), Kumamoto University (B6;D2-*Tg (CAG-EGFP) 49SImeg*; CARD ID: 267; http://cardb.cc.kumamoto-u.ac.jp/transgenic/strainsDetailAction.do?strainId=267). The background strain is C57BL/6. The *pCAG-eGFP* gene, illustrated in Supplementary Fig. 1A, was confirmed to be one copy by Southern blot analysis (Supplementary Fig. 1B). Expression of the *eGFP* gene is detected throughout the whole body.

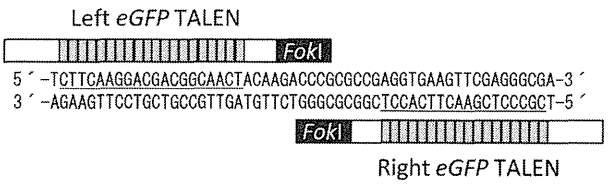

Fig. 1. Diagram depicting engineered TALENs binding to the *eGFP* gene. The TALENs comprise DNA-binding repeats (gray boxes), the N- and C-terminal domains of TALE (white boxes) and a *Fok*I nuclease domain (black box). The left and right TALEN target sequences are underlined.

To obtain mouse embryos for TALEN injections, C57BL/6N female mice were induced to super-ovulate using pregnant mare serum gonadotropin (PMSG; Serotropin; ASKA Pharmaceutical, Tokyo, Japan) and human chorionic gonadotropin (hCG; Veterinary Puberogen; Novartis Animal Health, Tokyo, Japan) at 5 weeks of age, and then mated with male *pCAG-eGFP* mice described above. Fertilized eggs were collected from females displaying vaginal plugs.

Microinjection of TALEN mRNAs

TALEN mRNAs were diluted in RNase-free PBS at 100 or 150 ng/μl for injection of each TALEN into the pronuclei or cytoplasm of zygotes. Approximately 2–3 pL of capped mRNAs was injected into the zygotes. The injected embryos were cultured in potassium simplex optimized medium with amino acids (KSOM-AA) at 37°C in 5% CO_2 and 95% humidified air for 1 h. Surviving embryos were transferred to the oviducts of pseudo-pregnant ICR female mice.

Genomic PCR for HMA and DNA sequencing

Genomic DNA was extracted from the tail of each pup using a DNeasy Blood & Tissue Kit (Qiagen). Genomic PCR was performed using LA *Taq* DNA polymerase (TAKARA Biotechnology, Shiga, Japan) under the following conditions: 94°C for 2 min; followed by 94°C for 30 s, 64°C for 30 s, and 72°C for 20 s for 38 cycles. The PCR primers were as follows: 5′-CCTCGTGACCACCCTGACCTAC-3′ and 5′-CTGTTGTAGTTGTACTCCAGCTTGTGC-3′. The PCR products were subjected to agarose gel electrophoresis and ethidium bromide staining for the HMA.

Table 1. TALEN-mediated eGFP gene disruption in mice

Route	Dose (ng/μl)	Injected	Transferred	Newborns	eGFP disappeared pups*	Analyzed pups	HMA	RFLP	Mutants
pronucleus	100	141	130	51 (39.2%)	3 (5.9%)	NT	NT	NT	NT
pronucleus	150	128	116	32 (27.6%)	4 (12.5%)	NT	NT	NT	NT
cytoplasm	150	80	69	33 (47.8%)	4 (12.1%)	33	12 (36.4%)	11 (33.3%)	17 (51.5%)
no injection	–	–	21	8 (38.1%)	0 (0%)	NT	NT	NT	NT

*Not including mosaic pups. HMA, heteroduplex mobility assay. RFLP, restriction fragment length polymorphism. NT, not tested.

For DNA sequence analysis, the PCR products were subcloned into pGEM-T Easy (Promega, Madison, WI, USA). The plasmids were extracted and sequenced using a T7 (5′-TAATACGACTCACTATAGGG-3′) or SP6 (5′-CATACGATTTAGGTGACACTATAG-3′) primer with a BigDye Terminator Cycle Sequencing Kit (Life Technologies), and then analyzed using an ABI PRISM 3130 Genetic Analyzer (Life Technologies).

RFLP analysis

The PCR products were purified using a Wizard SV Gel and PCR Clean-Up System (Promega). The purified products were digested with 3 units of *Acc*II (TAKARA Biotechnology), and then subjected to agarose gel electrophoresis and ethidium bromide staining.

Results and Discussion

As a model for TALEN-mediated knockout, we used fertilized eggs from mice ubiquitously expressing *pCAG-eGFP*. All of the fertilized eggs were heterozygous for the *pCAG-eGFP* gene. We selected the same *eGFP* TALEN target sequence as described previously [11] and newly constructed TALEN expression vectors as described in the Materials and Methods.

First, to judge the efficiency and toxicity between pronuclear and cytoplasmic injections, we microinjected *eGFP* TALEN mRNAs at 100 or 150 ng/μl into the pronuclei of zygotes. After the microinjection, 92.2% (130/141) and 90.6% (116/128) of the TALEN-injected embryos survived, respectively (Table 1). Following transfer of the surviving embryos to pseudopregnant females, 51 pups were born from 130 transferred embryos (39.2%) at 100 ng/μl and 32 pups were born from 116 transferred embryos (27.6%) at 150 ng/μl. Observation of the pups for green fluorescence under ultraviolet light on the day of birth revealed that eGFP fluorescence was completely abolished in three pups (5.9%) at 100 ng/μl and in four pups (12.5%) at 150 ng/μl (Table 1). The fluorescence images and DNA sequences of two of the three eGFP-disrupted pups at 100 ng/μl are shown in Fig. 2A and 2B, respectively. In addition, we obtained some pups with mosaic disruption of eGFP fluorescence at 150 ng/μl (Supplementary Fig. 2).

Next, *eGFP* TALEN mRNAs were injected at 150 ng/μl into the cytoplasm of zygotes. After the microinjection, 86.3% (69/80) of TALEN-injected embryos survived (Table 1) and 33 pups were born from 69 transferred embryos (47.8%). On the other hand, after transfer of *pCAG-eGFP* mouse embryos that had not been injected with TALEN mRNAs, eight pups were born from 21 embryos (38.1%). Thus, toxicity was not observed after the microinjection of TALEN mRNAs into the cytoplasm. When we observed the pups for green fluorescence under ultraviolet light, we found four pups in which fluorescence was completely absent and four mosaic pups (12.1% each) (Tables 1 and 2). Although the percentage of the green fluorescence-disappeared pups differed little from pronuclear injection, the birth rate of the pups with cytoplasmic injection was much higher than that with pronuclear injection (Table 1). Therefore, we concluded that TALEN mRNAs should be injected into the cytoplasm rather than the pronuclei. We then examined several analytical methods using the 33 pups described above.

Genomic DNA was extracted from all pups, and subjected to genomic PCR. The amplified product, including the TALEN target site, was 264 bp if no mutation was present. The individual products were subjected to agarose gel electrophoresis for the HMA. A recent study demonstrated that PCR products including TALEN-induced mutations could be detected by the HMA [9]. The HMA is the easiest method for the detection of mutations, because it only requires the performance of agarose gel electrophoresis after the genomic PCR. If mutations are introduced in the target DNA fragments, the shifted bands appear in proportion to the mutation rate based on the formation of heteroduplexes between the

Fig. 2. TALEN-mediated disruption of the *eGFP* gene in mice. (A) Bright-field (left panel) and fluorescence microscopy (right panel) images of newborn mice. *eGFP* TALEN mRNAs were injected into fertilized eggs heterozygous for *eGFP*. Embryos were transferred to pseudopregnant females. The arrowheads indicate pups in which *eGFP* is disrupted. (B) eGFP sequences in pups displaying a disrupted *eGFP* gene (M1 and M2). The original sequence is shown at the bottom with the TALEN target sequences (underlined). Deletions are indicated by dashes.

Table 2. Summary of the analyses for mutant screening

Founders	1	2	3	4	5	6	7	8	9	10	11
eGFP disruption	mosaic	ND	ND	ND	ND	ND	mosaic	ND	ND	ND	ND
HMA	+	ND	ND	ND	+	+	ND	ND	ND	ND	+
RFLP	+	ND	ND	ND	+	ND	ND	ND	ND	ND	+
Sequence mutation	NT	NT	NT	NT	NT	+	+	NT	NT	NT	NT
Genotype	MT				MT	MT	MT				MT
Founders	12	13	14	15	16	17	18	19	20	21	22
eGFP disruption	mosaic	ND	ND	ND	ND	ND	ND	ND	+	+	mosaic
HMA	+	ND	ND	ND	ND	+	ND	ND	+	ND	ND
RFLP	+	ND	+/–	ND	ND	+	ND	ND	ND	+	ND
Sequence mutation	NT	NT	+	NT	NT	NT	NT	NT	NT	+	+
Genotype	MT		MT			MT			MT	MT	MT
Founders	23	24	25	26	27	28	29	30	31	32	33
eGFP disruption	ND	ND	+	+	ND	ND	ND	ND	ND	ND	ND
HMA	+	+	ND	+	ND	ND	+	ND	+	ND	ND
RFLP	+	+	ND	ND	ND	ND	+/–	ND	+	ND	ND
Sequence mutation	NT	NT	+	NT	ND	NT	NT	NT	NT	NT	NT
Genotype	MT	MT	MT	MT			MT		MT		

HMA, heteroduplex mobility assay. RFLP, restriction fragment length polymorphism. ND, not detected. NT, not tested. MT, mutant.

mutated alleles and non-mutated alleles. We confirmed shifted bands in 12 pups (#1, 5, 6, 11, 12, 17, 20, 23, 24, 26, 29 and 31) (Table 2 and Supplementary Fig. 3). In two pups (#21 and 29), we detected PCR products of 264 bp and about 200 bp. These smaller bands suggested that extensive deletions were induced in these pups.

RFLP analysis is also often used for the detection of mutant alleles [1, 8, 15]. If there is a unique restriction site in the center of the TALEN spacer sequence, the mutated alleles obtain resistance to the restriction enzyme. The PCR products were purified from all individuals, and examined for whether they could be digested by *Acc*II. The original 264-bp PCR product is cleaved into two DNA fragments of 150 bp and 114 bp by *Acc*II digestion (Supplementary Fig. 4A). The PCR products of 11 pups (#1, 5, 11, 12, 14, 17, 21, 23, 24, 29 and 31) showed some resistance to *Acc*II, including less obvious ones such as #14 and 29 (Table 2 and Supplementary Fig. 4B). Although these results were similar to the HMA results (Supplementary Fig. 3), there were still some individuals that we could not confirm as mutants. Therefore, we determined the genomic *eGFP* sequences and expected amino acid sequences of such individuals (Supplementary Figs. 5A and 5B). Finally identified 17 pups as TALEN-mediated mutants (#1, 5, 6, 7, 11, 12, 14, 17, 20, 21, 22, 23, 24, 25, 26, 29 and 31; 51.5%) (Table 2).

The different results for the HMA and RFLP analysis were thought to be caused by the difference in the principles between these methods. If mutations are present that do not cause disruption of the recognition sequence of the restriction enzyme, they cannot be identified as RFLP-positive. On the other hand, a single base substitution or an extremely small insertion or deletion might not be detected by the HMA because of the minor effects on the heteroduplex mobility. In addition, some mice that were identified as mutants by HMA and/or RFLP analysis did not show the eGFP disruption (Table 2). There are some possible reasons of inconsistent results between green fluorescence observation and mutation analyses. One possibility is a failure of disrupting protein functions. If in-frame mutations or base substitutions are induced, green fluorescence could be remained. Another possibility is the timing of mutagenesis. If mutations are induced at late developmental stages, disruption of green fluorescence could be undetectable.

In summary, we assessed multiple analytical methods, comprising eGFP observation, HMA, RFLP analysis and DNA sequencing, for the detection of TALEN-induced mutants. Although DNA sequencing is generally the best way to definitely confirm mutations, it is very laborious work to subclone and sequence multiple clones for all pups. Although direct sequencing of genomic PCR products is easier than the above-described clone sequencing method, it can only detect mutations occurring at very early developmental stages. Considering all the various factors together, we think that there is a need to narrow down the candidates for mutants using the HMA and/or RFLP analysis before sequencing, even though it may lead to some mutant pups being overlooked, such as #25.

In contrast to other methods for analyzing TALEN-induced mutations that require specialized and costly equipment, such as high-resolution melting analysis [3] and surveyor nuclease assay [16], the methods that we tested require only commonly used reagents and equipment. We hope that this report will become a good model for the genotyping of TALEN-mediated knockout mutations, in mice and other organisms.

Acknowledgments

We thank Ms. Kazuko Kuroda and Ms. Reika Yoshimatsu for excellent technical assistance. Male *pCAG-eGFP* mice were kindly provided by Dr. Ken-ichi Yamamura at Kumamoto University. This study was supported by KAKENHI (24591016) to M. Ohmuraya from the Japan Society for the Promotion of Science.

References

1. Ansai, S., Sakuma, T., Yamamoto, T., Ariga, H., Uemura, N., Takahashi, R., and Kinoshita, M. 2013. Efficient targeted mutagenesis in medaka using custom-designed transcription activator-like effector nucleases. *Genetics* 193: 739–749. [Medline] [CrossRef]
2. Capecchi, M.R. 2005. Gene targeting in mice: functional analysis of the mammalian genome for the twenty-first century. *Nat. Rev. Genet.* 6: 507–512. [Medline] [CrossRef]
3. Dahlem, T.J., Hoshijima, K., Jurynec, M.J., Gunther, D., Starker, C.G., Locke, A.S., Weis, A.M., Voytas, D.F., and Grunwald, D.J. 2012. Simple methods for generating and detecting locus-specific mutations induced with TALENs in the zebrafish genome. *PLoS Genet.* 8: e1002861. [Medline] [CrossRef]
4. Davies, B., Davies, G., Preece, C., Puliyadi, R., Szumska, D., and Bhattacharya, S. 2013. Site Specific Mutation of the Zic2 Locus by Microinjection of TALEN mRNA in Mouse CD1, C3H and C57BL/6J Oocytes. *PLoS ONE* 8: e60216. [Medline] [CrossRef]
5. Joung, J.K. and Sander, J.D. 2013. TALENs: a widely applicable technology for targeted genome editing. *Nat. Rev. Mol. Cell Biol.* 14: 49–55. [Medline] [CrossRef]
6. Mashimo, T., Kaneko, T., Sakuma, T., Kobayashi, J., Kunihiro, Y., Voigt, B., Yamamoto, T., and Serikawa, T. 2013. Efficient gene targeting by TAL effector nucleases coinjected with exonucleases in zygotes. *Sci. Rep.* 3: 1253. [Medline] [CrossRef]